Journal of Geochemical Exploration 226 (2021) 106778

Contents lists available at ScienceDirect

Journal of Geochemical Exploration

journal homepage: www.elsevier.com/locate/gexplo

Base metal mobility linked to brine and hydrocarbon migration at the Huincul High in the Neuquén Basin, Argentina: Implications for the formation of sediment-hosted base metal deposits

M. Josefina Pons [a,b,c,*], Marta Franchini [b,d], Ana L. Rainoldi [b,e], Adolfo Giusiano [f], Nora N. Cesaretti [e,g], Aldo O. Montagna [a,h], Richard Herrington [i]

[a] Universidad Nacional de Río Negro, Río Negro, Argentina
[b] Consejo Nacional de Investigaciones Científicas y Técnicas, Centro Patagónico de Estudios Metalogenéticos, Argentina
[c] Instituto de Investigación en Paleobiología y Geología, UNRN-CONICET, Av. Roca 1242, 8332 Roca, Río Negro, Argentina
[d] Universidad Nacional del Comahue, Facultad de Ingeniería, Departamento de Geología y Petróleo, Buenos Aires 1400, CP8300, Neuquén, Argentina
[e] Dpto. de Geología, Universidad Nacional del Sur (UNS), Bahía Blanca, Argentina
[f] Consultant Geologist, CP:8300 Neuquén, Argentina
[g] CGAMA (CIC-UNS), San Juan 670, CP:8000 Bahía Blanca, Argentina
[h] YPF, S.A. Talero 360, Neuquén, Argentina
[i] Department of Earth Sciences, Natural History Museum, London, UK

ARTICLE INFO

Keywords:
Sediment hosted copper
Zinc and lead mineralizations
Basin architecture
Tectonic evolution

ABSTRACT

This contribution discusses the discovery of Pb—Zn mineralization in hydrocarbon exploration drill holes hosted in siliciclastic Jurassic rocks below the Cretaceous sediment hosted Cu mineralization located north of the Huincul High. In the Early Cretaceous, hydrocarbon and basinal water expulsion took place from the oil source rocks (Los Molles Formation) into the reservoir rocks Lajas Formation (Middle Jurassic), after the formation of diagenetic quartz overgrowths. Marcasite, pyrite and illite + illite-smectite mixed layer minerals then formed together with hydrocarbons. Marcasite ($\delta^{34}S$ −3.5 and −2.2‰) and pyrite ($\delta^{34}S$ −11.6 to 18.1‰) precipitated via bacterial sulfate reduction from fluids showing temperatures <80 °C and fluctuating pH conditions. During the Paleogene, Andean tectonism triggered migration of oxidized basinal brine containing dissolved leached Zn and Pb from the Los Molles Formation source rocks and S from the evaporites of the basin. This brine entered in the hydrocarbon reservoir of the Lajas Formation, resulting in the precipitation of sphalerite ($\delta^{34}S$ +10.4 to +10.8‰) and galena ($\delta^{34}S$ +5.2‰) by TSR at temperatures of 119–123 °C together with siderite. The Andean orogeny may also have triggered the migration of hydrocarbons + brines from the shallowest source rocks (Vaca Muerta Formation) and reservoir rocks (Mulichinco, Lajas and Lotena formations) into the red beds of the upper Cretaceous Neuquén Group, which became bleached as a result. Marcasite ($\delta^{34}S$ −36.4 to 18.2‰) and pyrite ($\delta^{34}S$ −60.2 to −24‰) precipitated by BSR, while calcite ($\delta^{13}C$ −12.3 to −5.6‰) formed due to redox reactions accompanying formation of quartz overgrowths, clay mineral coatings (δD −92.4‰ to −82.8‰ and $\delta^{18}O$ 16.2‰ to 18.40‰), and barite ($\delta^{34}S$ −5.9‰). Quartz overgrowths and barite precipitated from brines (1.5–10 wt% NaCl equiv.) at temperatures of 91–120 °C, with barite precipitating close to the feeder zones. Calcite cements are more widespread and generated from several pulses of brine and hydrocarbons up flow, evidenced by the wide range of homogenization temperatures (100–185 °C) and diversity of UV fluorescence colors of hydrocarbon-rich fluid inclusions. In subsequent Miocene tectonic events, basinal brines were able to leach Cu from the underlying thick red beds of the basin, entering the Neuquén Group oil reservoir traps or carrier beds where they became reduced. Chalcopyrite and bornite precipitated at temperatures >100 °C close to the feeder zones at the expense of barite as a local sulfur source. Chalcocite group minerals ($\delta^{34}S$ −21.3‰ to −7.3‰) precipitated outwards in pore spaces of the sandstones at lower temperatures (<100 °C) through BSR of sulfate in the mineralizing brines. Final exhumation of the Neuquén Group (Upper Miocene-Pliocene) promoted the infiltration of the meteoric water, the oxidation of the sulfides and formation of supergene Fe—Cu, V and U minerals. Isotope geochemistry and fluid inclusion results combined with alteration and ore mineralogy document the processes controlling the

* Corresponding author at: Universidad Nacional de Río Negro, Río Negro, Argentina.
E-mail address: jpons@unrn.edu.ar (M.J. Pons).

https://doi.org/10.1016/j.gexplo.2021.106778
Received 19 August 2020; Received in revised form 4 March 2021; Accepted 14 March 2021
Available online 31 March 2021

distribution of base metals in the Huincul High region that can be applied to evaluate the metal potential in other areas of the Neuquén Basin and further extrapolated to similar geological systems elsewhere.

1. Introduction

The Neuquén Basin is a complex back arc-foreland basin developed eastward of the Andean Cordillera (Argentina) (Fig. 1A). During the Late Triassic-Early Jurassic the basin formed as a rift system followed by several episodes of structural inversion (Ramos and Kay, 2006). This tectonic evolution is reflected in the 220 Ma stratigraphic record of basin subsidence with 7000 m of preserved Upper Triassic-Cenozoic basin infill of marine, evaporite, continental sedimentary and volcanic rocks together the development of hydrocarbon source and reservoir rocks (Uliana and Legarreta, 1993).

The Neuquén Basin architecture favored the development of Pb—Zn mineralization in the Jurassic dolomitic and siliciclastic facies of the Cuyo Group and Cu mineralization in the Cretaceous red beds of the Neuquén Group, all spatially associated with bitumen. Most of the deposits are located above the major structures and hydrocarbons fields of the basin (Fig. 1A; Giusiano et al., 2006, Giusiano et al., 2008; Pons et al., 2009; Pons et al., 2015; Rainoldi et al., 2015; Paz et al., 2016; Pons et al., 2017; Rainoldi et al., 2019). Recent studies of sediment hosted Cu deposits (SHCD) of the Neuquén Basin (Giusiano et al., 2006, 2008; Pons et al., 2009; Pons et al., 2015; Pons et al., 2017; Rainoldi et al., 2015; Rainoldi et al., 2019) propose a hypothesis that links Cu mineralization with hydrocarbon and Cu-bearing brine migration along brittle structures of the Huincul High and Los Chihuidos High. Rainoldi et al. (2019) presented the first isotopic and fluid inclusion study of two SHCD located in the southern zone of Huincul High (El Porvenir) and at Los Chihuidos High (Fig. 1A–B) that provides evidence for the interaction of hydrocarbons and formation water with host red beds and metal-bearing basinal brines. These Cu deposits share some similarities with the deposits of the Paradox Basin, Colorado (USA, Hitzman et al., 2005) yet show clear differences in the nature and role of the metal reductant at the deposit scale (Rainoldi et al., 2019).

Zinc and lead sulfides hosted in dolomitic facies of the Lajas Formation (Puesto Gregor; Fig. 1A) at the Huincul High were first reported by Garrido et al. (2000) who attribute an epigenetic origin for the mineralization. In other regions of the Neuquén Basin de Barrio et al. (2014), Escobar (2016) and Salvioli (2017) describe Zn—Pb mineralization associated with barite and celestine hosted in the Mesozoic

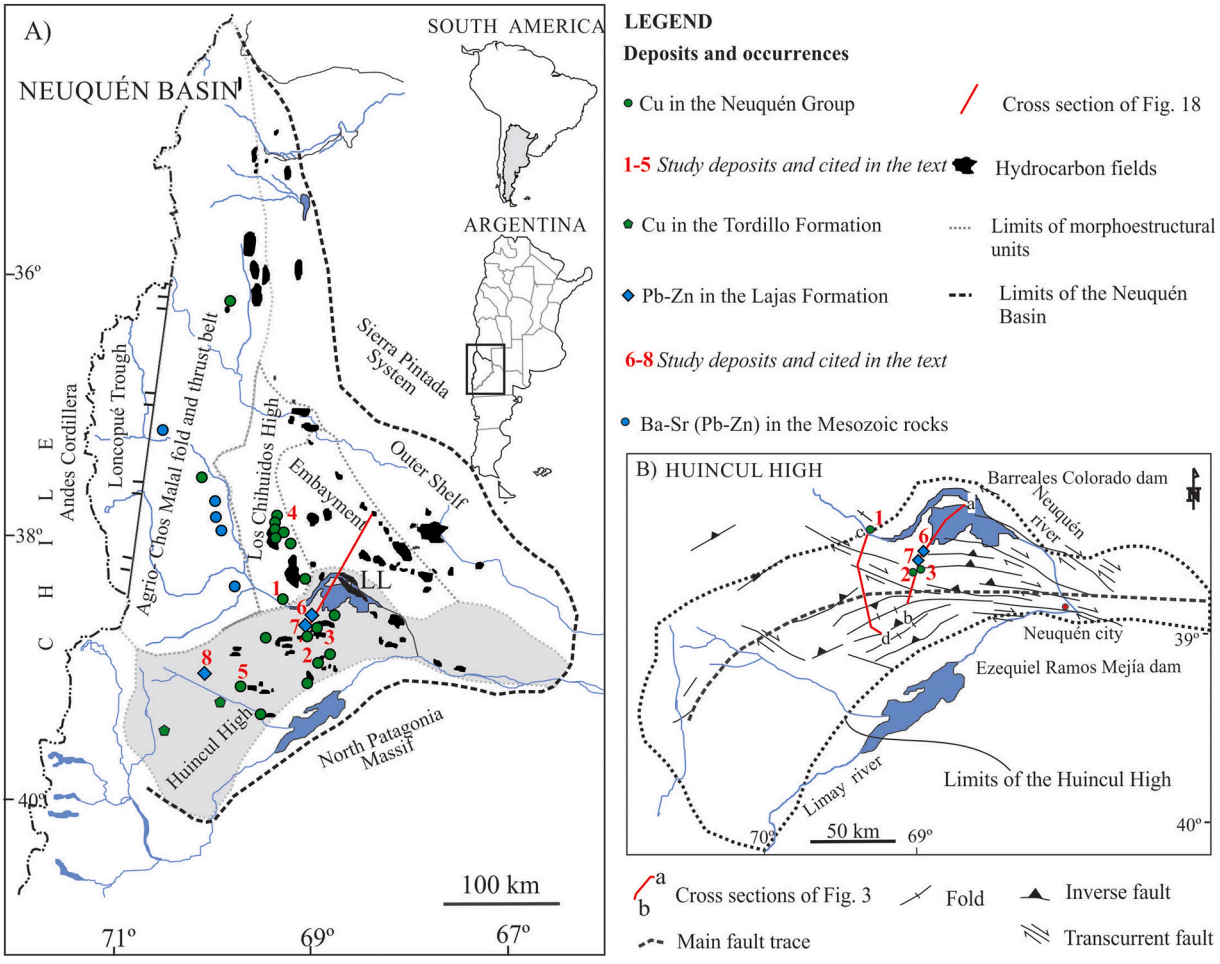

Fig. 1. A) Neuquén Basin and its main morphostructural units showing the distribution of hydrocarbons fields (black) and the main sediment hosted copper deposits (1: Tordillos, 2: Barda González, 3: La Cuprosa, 4: Los Chihuidos, 5: El Porvenir), the zinc and lead (6: Cupén Mahuida, 7: Aguada Baguales, 8: Puesto Gregor) and some of the Ba—Sr (Zn—Pb) deposits and occurrences (modified from Giusiano et al., 2008; de Barrio et al., 2014). The red line indicates the position of the cross section shown in Fig. 17. B) Detailed map of the Huincul High with the main structures (modified from Silvestro and Zubiri, 2008) and the location of the 1: Tordillos and 2: Barda González deposits and 3: La Cuprosa, 6: Cupén Mahuida and 7: Aguada Baguales occurrences. Red lines show the location of the cross sections of Fig. 3. (For interpretation of the references to color in this figure legend, the reader is referred to the web version of this article.)

evaporitic and carbonate sequences (Fig. 1A) and the authors interpret these as either MVT or Sedex type deposits.

The Barda González, La Cuprosa and Tordillos (Fig. 1A–B) are SHCD located on the main structure of the Huincul High and in its northern sector, in the Barda González, Aguada Baguales and Ricón del Mangrullo oil fields, respectively. The Barda González-La Cuprosa deposits have a total inferred resource of 36.33 Mt with average grade of 0.37% Cu and Tordillos contains 9.5 Mt with average grade of 0.45% Cu (Lyons, 1999; Zientek et al., 2015) with anomalous Mo, V, U, Ag, Zn and Pb (Testi, 2006; Pons et al., 2015). Zinc and Pb mineralization have also been discovered at Aguada Baguales and Cupen Mahuida hydrocarbon fields, close to the Barda González-La Cuprosa SHCD (Fig. 1A–B). Sulfides of Zn and Pb occur in the fluvio-deltaic Aalenian-Bajocian rocks of the Lajas Formation (Fig. 2) one of the most important tight sandstone gas reservoirs of the Neuquén Basin (Raggio et al., 2014).

In this paper we propose to explain the role of hydrocarbons and metal-bearing basinal brines in the genesis of SHCD and Zn—Pb sandstone hosted mineralization in the northern block of the Huincul High. This explanation is based on petrographic descriptions and new geochemistry data that is complemented by fluid inclusion and stable isotope analyses of diagenetic and alteration minerals and hypongene sulfides hosted in the Mesozoic sedimentary sequences of the Neuquén Basin. Outcrop and drill core samples were taken from a range of depths and horizontal distances from the main fault structures (Huincul High; Fig. 1A–B).

2. Geologic setting and ore host rocks

2.1. Geology of the Neuquén Basin

The Neuquén Basin is a poly-phase basin developed on Late Proterozoic to Late Paleozoic basement rocks (Fig. 2), comprising low-grade

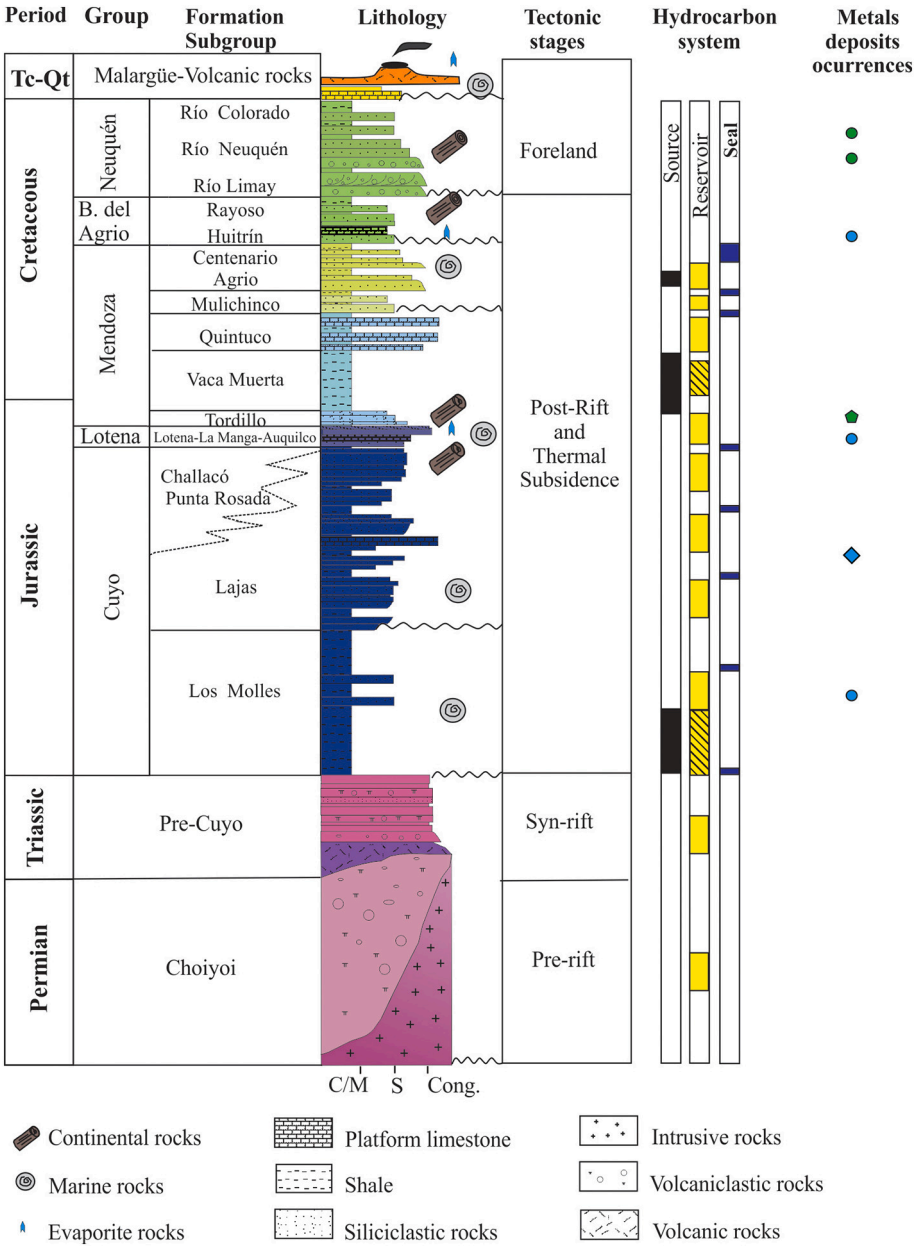

Fig. 2. Chronostratigraphic column of the Neuquén Basin at the Huincul High region (modified from Malone et al., 2002; Ostera et al., 2016) with the main tectonic stages. The main source, hydrocarbon reservoirs, and seal rocks are shown along with the Cu, Zn—Pb, Ba—Sr with minor Zn—Pb mineralizations. References for metal deposits — occurrences are shown in Fig. 1. C/M: claystone/mudstone, Cong: conglomerate, Qt: Quaternary, S: sandstone, Tc: Tertiary.

metamorphic and plutonic-volcanic rocks that are the products of terrane accretion and arc magmatism in the western margin of Gondwana (Charrier et al., 2007). The stratigraphy of the basin reflects its geodynamic history (Howell et al., 2005; Ramos and Kay, 2006; Mosquera and Ramos, 2006) and consists of sedimentary and volcanic deposits belonging to the Pre-Cuyo, Cuyo, Lotena, Mendoza, Bajada del Agrio, Neuquén and Malargüe Groups (Fig. 2).

The first episode of sedimentation in the Neuquén Basin is represented by volcanic, volcaniclastic and clastic rocks of the Pre-Cuyo Group deposited in isolated half-grabens. The Cuyo Group (Pliensbachian-Callovian; Riccardi, 2008) records the first marine ingression that crossed the cordilleran axis (Vicente, 2005, 2006). The progressive transgression flooded most of the early *syn*-rift deposits and covered the Neuquén Embayment with organic claystones and mudstones of the Los Molles Formation. The fluvial deltaic sandstone and conglomerate of the Lajas Formation overlay the organic mudstones and represent the regression of the system (Goméz et al., 2017) that culminated with fluvial and evaporite-bearing rocks (Punta Rosada, Challacó and Tábanos formations).

The second transgressive–regressive cycle is represented by the Lotena Group (Callovian-Oxfordian; Groeber, 1946; Leanza, 1992; Vergani et al., 1995). This group includes continental sandstone and clastic platform facies of the Lotena Formation, followed by marine carbonate facies of the La Manga Formation and culminated with a thick evaporite sequence of the Auquilco Formation. These carbonate and evaporite units are less developed in the marginal zones of the Neuquén Basin such as in the Huincul High region.

The Kimmeridgian-Barremian deposits of the Mendoza Group (Legarreta and Uliana, 1999) comprises initial red beds sequences of coarse conglomerate, fluvial alluvial, lacustrine and aeolian sandstone, and volcaniclastic deposit of the Tordillo Formation (Kimmeridgian-Early Tithonian; Legarreta and Uliana, 1999). Black shale facies of the Vaca Muerta Formation (Tithonian-Early Valanginian) were deposited during a sea-level rise phase (Leanza, 1973; Leanza et al., 2011). The sea regression is represented by the clastic limestone deposits of the Quintuco Formation (Casadío and Montagna, 2015) followed by a sharp sea-level drop during the Late Valanginian leading to deposition of continental, mixed, and marine siliciclastic facies of the Mulichinco Formation, in the central part of the basin (Schwarz and Howell, 2005). A thick sequence composed of black shale, carbonate, and continental sandstone facies belonging to the Agrio Formation (Late Valanginian-early Barremian) were deposited.

The Bajada del Agrio Group (Leanza, 2003; Leanza et al., 2005) represents the final drying stage of the basin conformably deposited on the Mendoza Group rocks. Sedimentation began again with a stage of continental basin sedimentation represented by aeolian fluvial deposits and shallow marine sequences (evaporitic-carbonate deposits) of the Huitrín Formation. During the Aptian to Albian, a final disconnection of the Neuquén Basin from the paleo-Pacific Ocean led to deposition of the clastic–evaporitic sequence of the Rayoso Formation (Leanza, 2003). By the Early Cretaceous the back-arc sag phase was complete, and the tectonic regime changed to being compressive in the southern Central Andes (Ramos, 2010) with eastward migration of the orogenic front and consequently, the Neuquén Basin began to form the foreland (Zamora Valcarce et al., 2006; Tunik et al., 2010).

During the Cenomanian, westward contraction of the Agrio and Chos Malal fold-and-thrust belt (Fig. 1A) produced the low-angle intra-Cenomanian unconformity at the top of the Bajada del Agrio Group, with the deposition (1300 m) of Late Cretaceous synorogenic fluvial-lacustrine and aeolian red beds of the Neuquén Group which can be subdivided into seven formations (Ramos, 1981). The Malargüe Group composed of several distinctive formations is separated from the Neuquén Group by an erosional unconformity. One of the main stratigraphic features of the group is the record of the first Atlantic marine ingression into the basin during Maastrichtian–Danian times (Aguirre-Urreta et al., 2011).

All these regional transgressive–regressive cycles controlled the configuration of the Neuquén Basin and favored the development of oil and gas source reservoir and seal rocks (Fig. 2; Schiuma et al., 2002; Legarreta et al., 2003; Villar et al., 2005) leading to condition favorable to form the most important hydrocarbon fields of Argentina (Uliana and Legarreta, 1993; Schiuma et al., 2002).

Intraplate deformation in the Neuquén Basin has been active since the Early Jurassic and has varied in intensity and location, resulting in a complex mosaic of modern morphostructural units: Chos Malal and Agrio fold and thrust belt, Loncopué Trough, Huincul High, Los Chihuidos High, Embayment and Outer Shelf (Mosquera and Ramos, 2006; Fig. 1A). SHCD are widely distributed throughout the basin, but the best examples are placed in the Huincul High region (Fig. 1A). The Huincul High is a structural lineament of regional scale developed at 39° south latitude, with east–west strike that extends 270 km (Fig. 1B), defining the northern boundary of Argentinean Patagonia with the Neuquén Basin (Ramos et al., 2004). This structure has been interpreted as a dextral fault zone with both transpressive and transtensive segments due to changes in the fault zone trend (Ploszkiewicz et al., 1984). Silvestro and Zubiri (2008) proposed that the High resulted from of an oblique northwest–southeast convergence during the Early Jurassic and Cretaceous. Compressive events continued up to Pliocene and produced new structures and reactivated some of the previous rift system developed between the North Patagonian Massif in the southeast and the Neuquén Basin in the northwest (Cruz et al., 2002; Silvestro and Zubiri, 2008). Most of these faults are deep-seated but die out at the base of the Vaca Muerta Formation (Tithonian; Fig. 3A–B). Other faults closer to the main fault originate in shallower depths, cross-cutting the base of the Neuquén Group (Schiuma et al., 2002; Silvestro and Zubiri, 2008; Fig. 3A–B).

In the area of the Huincul High, at the Aguada Baguales and Cupen Mahuida anticline oil fields, the productive horizons correspond to the Cuyo and Lotena Groups (Figs. 2, 3A–B; Schiuma et al., 2002; Coppo et al., 2018). The hydrocarbon trap consists of truncations against the regional seal (Vaca Muerta Formation) on the north flank of an E-O anticline (Fig. 3A–B). However, on the ridge of this structure, erosion of the seal allowed migration of hydrocarbons to shallower levels (Intravalanginian discordance, Fig. 3A–B; Cevallos, 2005). North of the Huincul High region there is a spatial correlation between main faults systems, hydrocarbon fields and both Zn—Pb mineralization hosted in the Lajas Formation in subsurface and stratiform Cu deposits in the Neuquén Group (Giusiano et al., 2008; Fig. 1B).

2.2. *Zn—Pb mineralization*

Zinc-Pb mineralization is hosted in the Lajas Formation. At the Huincul High this unit has only been recognized in the subsurface where it overlies the Los Molles Formation and is covered by the Lotena or the Vaca Muerta formations (Figs. 3A, 4A–B). At the Aguada Baguales oil field, AB1 well (Fig. 3A) intersected the Lajas Formation between 970 and 1088 m below surface and Zn—Pb mineralization is hosted mainly in the paleo-channel lithofacies (Fig. 4A) characterized by lithic and lithic feldspathic conglomerate and sandstone. The porosity of these facies varies from 9.4 to 17%, depending on the degree of diagenetic minerals occlusion of the pore spaces (Aguirre et al., 1997). These rocks show a moderate to high content of light oil and solid hydrocarbons with yellow and black/brown colors, respectively. Four pre-mineralization stages of porosity infill were recognized (Fig. 5): 1) early gypsum-anhydrite (Fig. 6A), 2) quartz overgrowths 10–100 μm thick rimmed by hydrocarbon (Fig. 6B), 3) marcasite and 4) illite (illite-smectite mixed layer minerals) (Fig. 6D–E).

At the Cupen Mahuida oil field located 11 and 13 km north of the main structure of the Huincul High, the C-1, C-2, C-3, C-4 wells from the YPF oil company intercepted the Lajas Formation at depths between 1561–1758 and 2540–3053 m (Fig. 3A). At this zone, the Lajas Formation is dominated in its lower section by fluvio deltaic facies and grade upward (middle and upper sections) to distributary channels facies

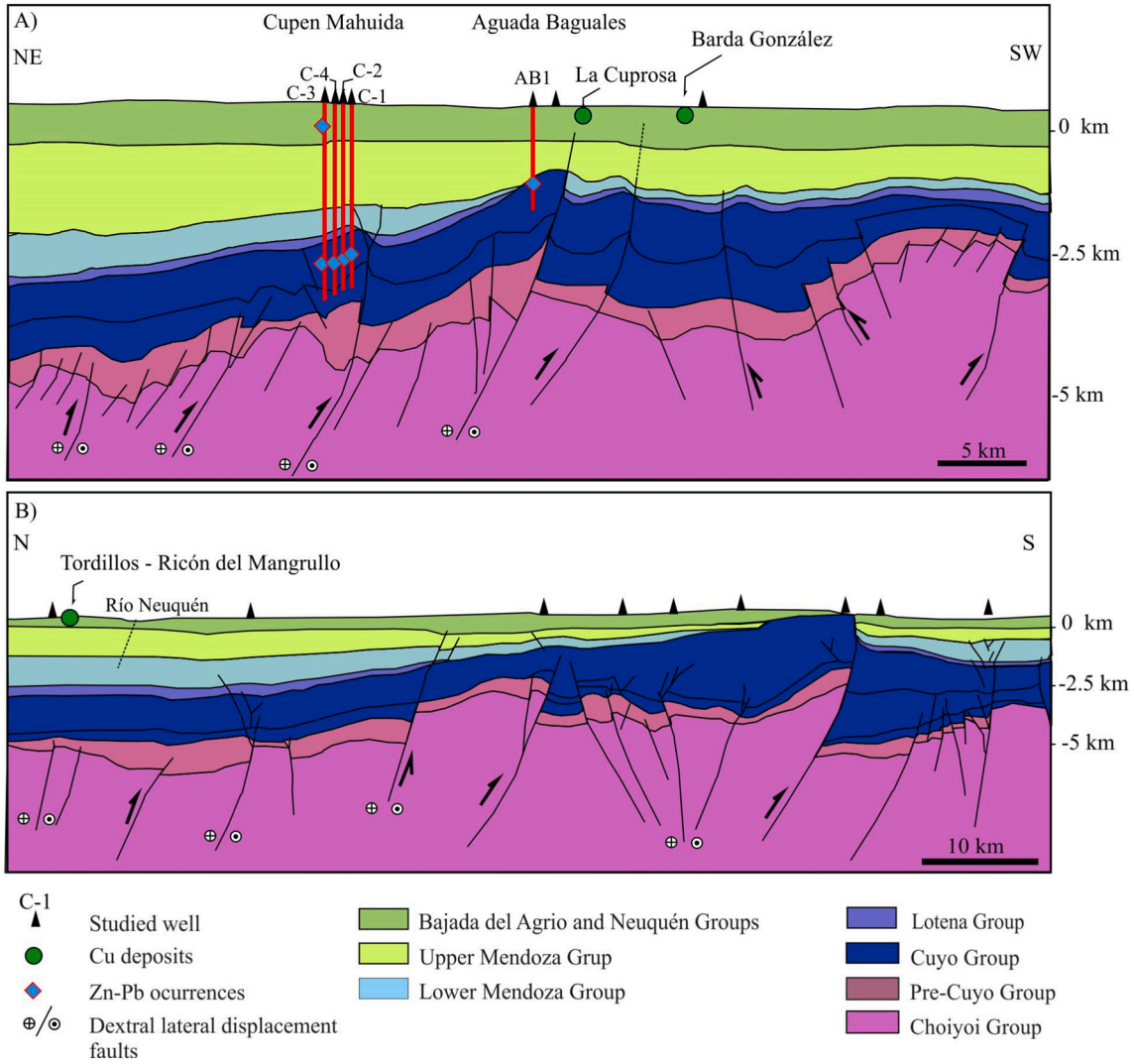

Fig. 3. Cross sections at A) Aguada Baguales, Cumpen Mahuida, and B) at Rincón del Mangrullo oil fields (modify from Silvestro and Zubiri, 2008) showing the location of the studied SHCD and Zn, Pb, Cu occurrences.

associated to distal deltaic plain deposits (Coppo et al., 2018). In all wells the coarsest facies show similar detrital composition described above for the sandstone at Aguada Baguales but with lower porosity (<10%; Montagna et al., 2017; Coppo et al., 2018). Authigenic minerals identified are quartz overgrowths with bitumen coating, euhedral pyrite, illite-smectite mixed layers as both grain coatings and as replacement of feldspar and lithic clasts, and later siderite. Zinc-lead occurrences were also intercepted in well C-3, at depths between 420 and 430 m at the base of the Huincul Formation (Figs. 3A, 4B). The diagenetic minerals in the Huincul Formation are characterized by quartz overgrowths with hydrocarbon impregnations coating grains, euhedral pyrite, framboidal pyrite, and smectite with smectite-illite mixed layers coating detrital grain surfaces and replacing mud chips and lithic fragments.

2.3. Cu mineralization

Copper mineralization is hosted in the Huincul and Portezuelo formations of the Neuquén Group (Figs. 3A–B, 4B). These rocks were originally red, but at the site of mineralization they have become bleached (Fig. 4B; Pons et al., 2009; Rainoldi et al., 2015; Paz et al., 2016; Pons et al., 2017; Rainoldi et al., 2019). Bleaching and mineralization occur mainly in moderately to well sorted litharenite, feldspathic litharenite and conglomerate layers. Pons et al. (2009, 2015, 2017) and Paz et al. (2016) describe the textural variability and complex mineral paragenesis of the unaltered red beds and altered rocks at Tordillos and Barda González deposits and La Cuprosa prospect. The last two mineralized zones are treated together due to their similarities (host rocks, proximity, diagenesis, alteration, and ore mineralogy).

At Tordillos, early diagenetic minerals like hematite, kaolinite, calcite 1 (Figs. 5, 6F) and traces of barite 1 coating have been preserved only in the red-brown mudstone. In the thickest paleochannel of the Huincul Formation, dissolution of early cements and clasts has increased the porosity up to 24%, sandstone and conglomerate units have changed color from red to white, greenish gray and gray due to the leaching of hematite (bleaching) (Pons et al., 2017). Bitumen impregnations are abundant along with multistage calcite (2, 3 and 4; Fig. 6H–I) framboidal-pyrite, montmorillonite, quartz overgrowth, and coarse grained barite 2 (Table 1), forming tubes and flames. Gray and greenish gray sandstones with montmorillonite + V bearing-hematite and chlorite-smectite mixed layers (chlorite) + calcite 4 ± micro quartz overgrowth + pyrite (Figs. 5, 6I–J), respectively occur along the redox front between the red-brown mudstone and the white sandstone and conglomerate (Pons et al., 2017).

At Barda González-La Cuprosa, early diagenetic iron oxide and hydroxide cements are only preserved in the less permeable claystone and

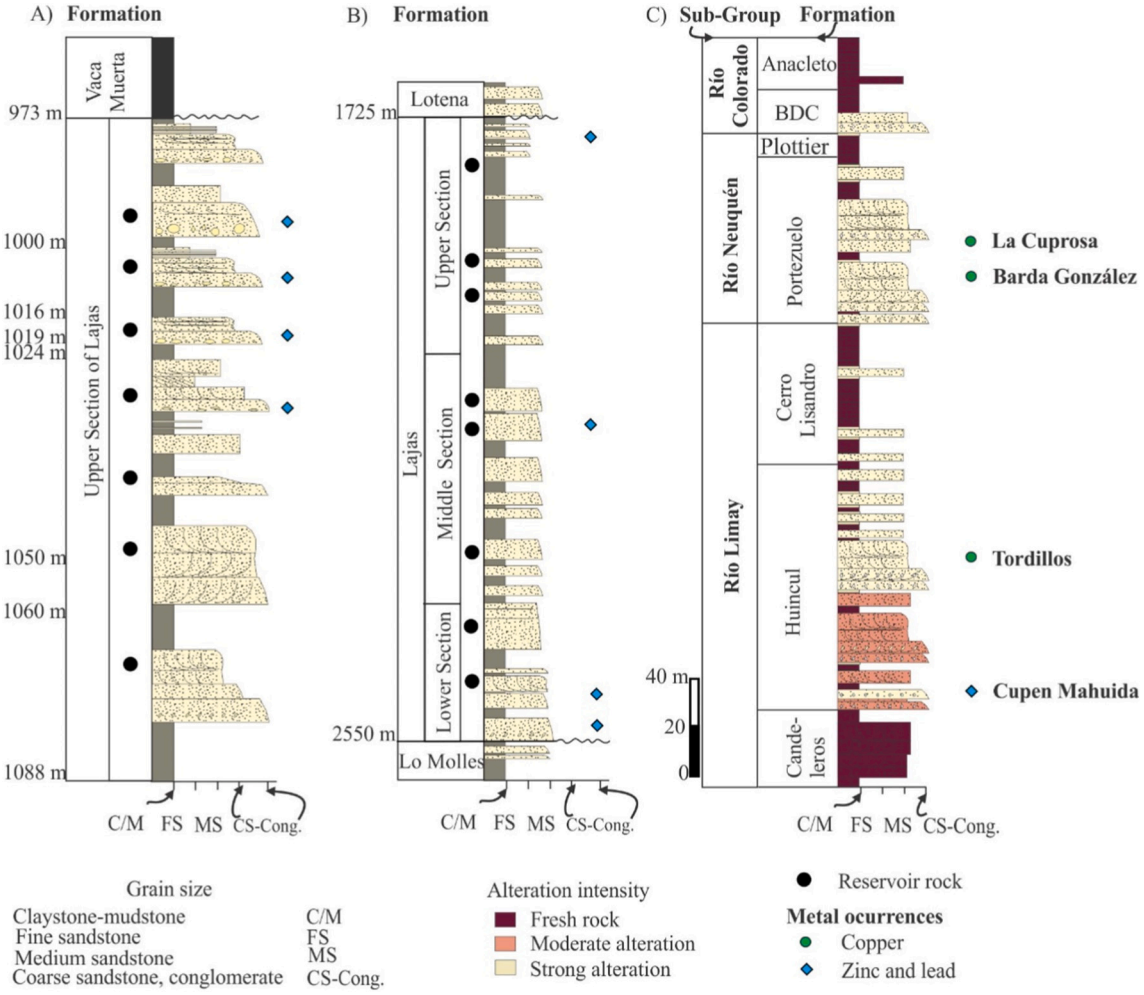

Fig. 4. Stratigraphic columns. A) Upper section of the Lajas Formation (modified from Aguirre et al., 1997) at Aguada Baguales. B) The Lajas Formation (modified from YPF oil company internal report) at Cupen Mahuida hydrocarbon fields. C) The Neuquén Group at the Huincul High region (modify from Giusiano et al., 2008).

mudstone layers of the Portezuelo Formation (Pons et al., 2009; Pons et al., 2015; Paz et al., 2016). Paleo-migration of hydrocarbons and formation waters along the most permeable sandstone and conglomerate have bleached the rocks with partial to total dissolution of both, grains and early cements (hematite, calcite), thereby increasing the porosity up to 26% (Pons et al., 2015; Paz et al., 2016). The reaction of hydrocarbons and brines with host rocks formed the following authigenic minerals (Fig. 5): (1) micro quartz overgrowths, montmorillonite and disseminated pyrite in the medium- to fine-grained sandstone and mudstone (Fig. 6J), (2) traces of barite and pyrite in the coarse-grained sandstone and conglomerate and (3) multistage calcites (Fig. 6K, L; Pons et al., 2009; Pons et al., 2015 and Paz et al., 2016). Bitumen coats the grains and fractures and is associated with calcite 3 and calcite 4 (Fig. 6J–L), cutting both calcite 1 and 2 (Fig. 6L). Analcime veins cut previous calcites (Fig. 6L). Close to the contact with the Cerro Lisandro Formation, the mudstone of the Portezuelo Formation contains marcasite and pyrite in contact with bitumen (Pons et al., 2015). Late calcite 5 fills fractures and open spaces (Fig. 6L).

3. Analytical methods

Bleached, fresh, and mineralized sandstone samples were collected from outcrops distributed along 5 and 4 stratigraphic columns of the Huincul Formation (n = 5) at Tordillos (n = 120) and of the Portezuelo Formation (n = 4) at Barda González-La Cuprosa (n = 182), respectively. Available drill cutting samples were collected from the Barda González deposit (n = 94), the Cupen Mahuida (n = 106) oil field, and from drill core samples (n = 6) from the Aguada Baguales oil field. All samples have been studied by binocular microscope with selected samples (107 thin sections) analyzed using a polarizing microscope under both transmitted and reflected light.

Double polished thin sections wafers of sandstones containing quartz, calcite, barite, siderite, sphalerite and analcime cements were selected for fluid inclusions study. They were analyzed petrographically using a polarization fluorescence Nikon Eclipse 50i Pol microscope of the Laboratorio de Luminiscencia of the Departamento de Geología at Universidad Nacional del Sur, Bahía Blanca, Argentina. The fluid inclusion assemblage (FIA) and the classification (primary, pseudosecondary and secondary) are made following Goldstein and Reynolds (1994). Micro thermometric analysis was performed using a Linkam MDS 600, (−180°/+600 °C) fluid inclusion heating and freezing stage mounted on a Olympus petrographic microscope with BX50 and Leitz UTK50/0.63, at the Laboratorio de Inclusiones Fluidas of the Departamento de Geología, Universidad Nacional del Sur. Salinities were calculated directly converting the final ice meting temperature (°C) obtained from aqueous two-phase fluids inclusions into wt% NaCl equiv. using the equation for H_2O-NaCl system of Bodnar, 1992.

Sulfides, sulfates, carbonates, bitumen and clay minerals were separated (handpicking, microdrilling and extracted sedimentation) for sulfur, carbon, oxygen and hydrogen isotope analyses at the Servicio de Isótopos Estables, Universidad de Salamanca, Spain and at the Scottish Universities Environmental Research Centre (SUERC), East Kilbride,

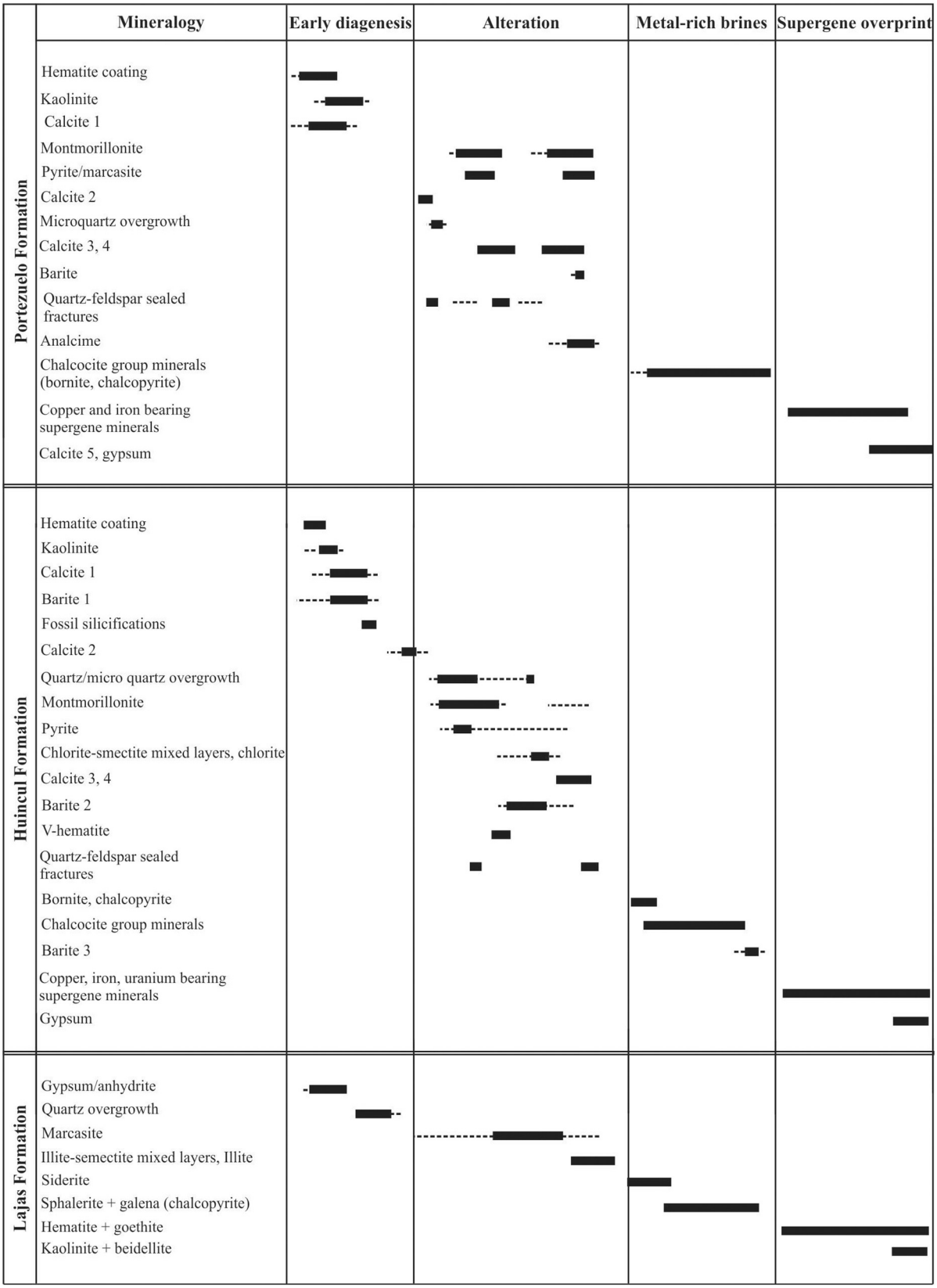

Fig. 5. Paragenetic sequence of porosity infill minerals from the Lajas, Huincul and Portezuelo formations.

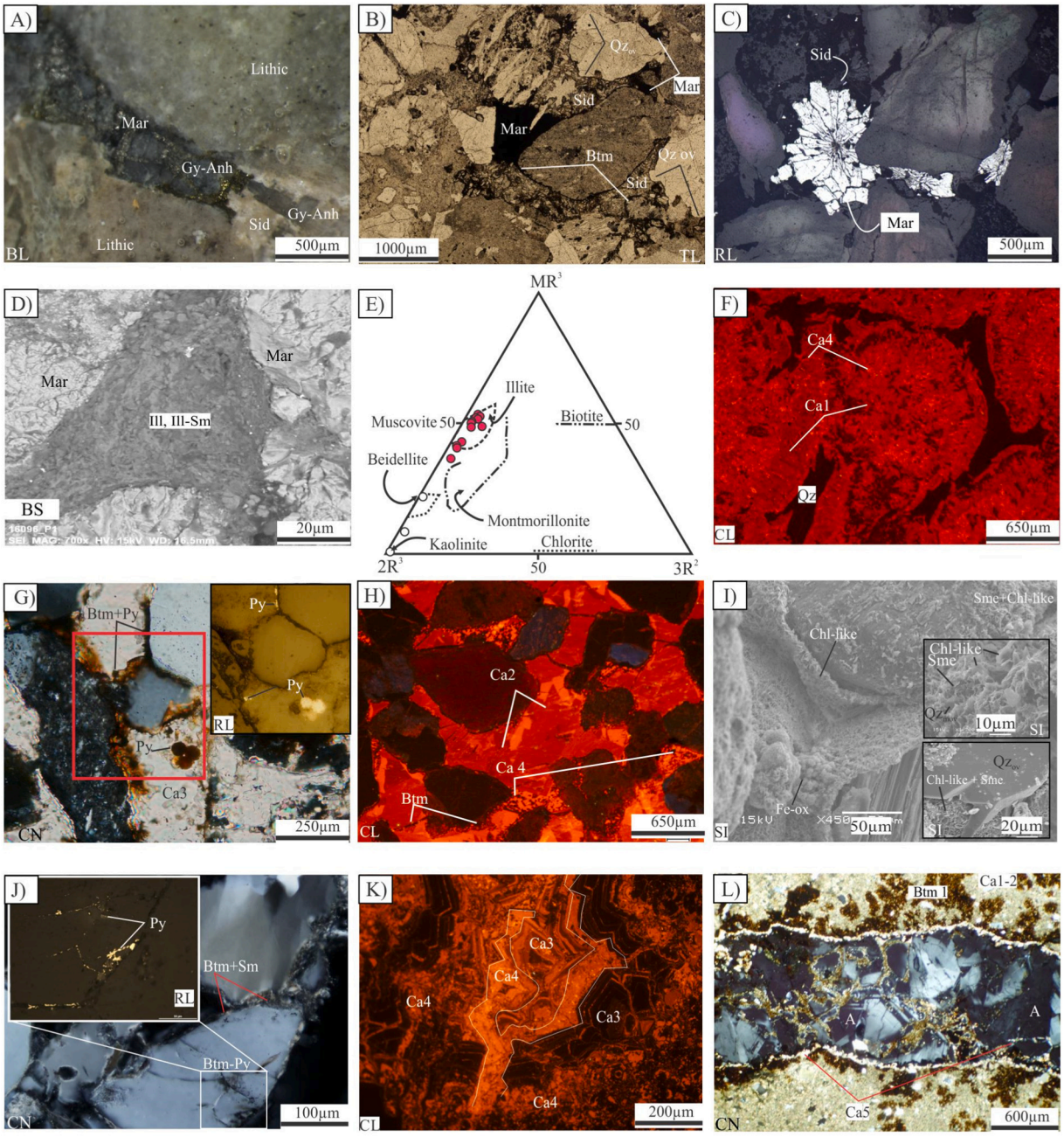

Fig. 6. Microphotographs of diagenetic and alteration minerals of the Lajas Formation. A) Early gypsum-anhydrite cement partially replaced by marcasite. B) Bitumen coating grains and quartz overgrowth in contact with fibrous radial marcasite and euhedral siderite filling the remaining porosity. C) Interstitial fibrous radial marcasite. D) Back scattered electron image of marcasite and illite + illite-smectite mixed layers cements. E) Plot of the clay mineral compositions in the MR^3–$2R^3$–$3R^2$ triangle, in which silica is considered as a component in excess, $MR^3 = Na + K + 2Ca$. $2R^3 = ([Al + Fe^{3+}] - MR^3) / 2$, and $3R^2 = (Mg + Mn + Fe^{2+}) / 3$ (Velde, 1985. F–I) Photomicrographs of diagenetic and alteration minerals of the Huincul Formation. F–H) Multistage carbonate cements, G) Calcite 3 cement including framboidal pyrite and bitumen impregnations in the white sandstone. I) Smectite, chlorite-smectite mixed layers and chlorite coating grains in the greenish gray sandstone. J–L) Photomicrographs of diagenetic and alteration minerals of the Portezuelo Formation. J) Bitumen + smectite grain coating and pyrite + bitumen filling grain fractures in the white sandstone. K) Calcite 3 and 4 cements in the white sandstone. L) Early calcite 1–2 cement cut by bitumen and analcime vein and late calcite 5. Type of images: BL: obtained with binocular microscope, BS: Back scattered electron, CL: cathodoluminescence, CN: polarized microscope with transmitted light with crossed nicols, RL: with reflected light, SI: SEM; TL: with transmitted light. A: analcime, Btm: bitumen, Ca: calcite, Chl: chlorite, Gy-Anh: gypsum-anhydrite, Ill-Sm: illite smectite mixed layers, Mar: marcasite, Mqzov: micro quartz Qz_{ov}: quartz overgrowth, Sid: siderite, Sm: smectite, Sm-chl: smectite-chlorite mixed layers.

Glasgow, Scotland using a VG Isotech SIRA II gaseous source dual inlet, AP 2003 and VG Optima mass spectrometers. Separation of the sulfur of three samples with copper sulfides and barite cements was carried out following the chemical extraction method (Hall et al., 1988).

Due to the complexity of carbonate cements, zones dominated by one or two types of calcite (calcite 1, 2, 3–4 and calcite 5) were selected after a petrographic and cathodoluminescence study and sampled by microdrilling. Prior to the isotope analyses of carbonate, a heater Asher model K1050X EMITEC was used to eliminate traces of bitumen and organic matter combusting these at low temperature in the presence of oxygen plasma. CO_2 for isotopic analysis was produced by reaction with 100% H_3PO_4 (McCrea, 1950) and SO_2 was produced by reaction of the sulfide

Table 1
$\delta^{18}O$ and δD isotopic data of clay minerals from the altered sandstone and current reservoir water.

Sample	Formation	Fraction (μm)	Type of sample	Mineral	$\delta^{18}O_{V\text{-}SMOW}$	$\delta D_{V\text{-}SMOW}$
To 111209-16	Huincul	<2 μm	Bleached S.	Sm	+17.6	−87.50
To 11108-7d	Huincul	<2 μm	Bleached S.	Sm	+17.4	−92.40
To 140209-6-2	Huincul	<2 μm	Bleached S.	Sm	+18.4	
To 140209-6	Huincul	<2 μm	Bleached S.	Chl + Chl-Sm	+18.3	−82.8
To 111209-7	Huincul	<2 μm	Bleached S.	Chl + Chl-Sm	+16.2	−85.20
Reservoir water*	Lajas		Water		−4.65	−37.50

S: sandstone; Sm: smectite; Chl: chlorite; Chl-sm: chlorite-smectite mixed layers. Analyzed at the Servicio de Isótopos Estables, Universidad de Salamanca.
* Scottish Universities Environmental Research Centre.

or sulfate minerals with an oxidant (Cu_2O) at elevated temperature (1000 to 1200 °C) under vacuum (Hair et al., 1973; Coleman and Moore, 1978). Average reproducibility by the chosen methods was better than ±0.02‰ for $\delta^{13}C$ and ±0.12‰ for $\delta^{18}O$ in carbonates, ±0.2‰ for $\delta^{18}O$ by laser fluorination in clay minerals, ±1‰ for δD, and ±0.1‰ for $\delta^{34}S$ in sulfides and sulfates. In situ laser S isotope analyses were implemented following Kelley and Fallick (1990) and Wagner et al. (2002). Liberated and purified gases were analyzed on a VG Isotech SIRA II mass spectrometer and standard corrections applied to produce true $\delta^{34}S$ (including correction for the small laser-induced isotopic fractionation, as listed in Wagner et al., 2002). The international standards used were NBS-123 and IAEA-S-3, and SUERC standard CP-1. These give $\delta^{34}S$ values of +17.1‰, −31.5‰ and −4.6‰ respectively, with 1σ reproducibility around ±0.2‰. For isotopic analyses of clay minerals, we follow the methodology explained in Rainoldi et al. (2019), oxygen and hydrogen were measured with VG SIRA 10 mass spectrometer and VG Optima mass spectrometer, respectively. Isotopic results are reported in δ notation as per mil (‰) deviations relative to V-SMOW (Vienna Standard Mean Ocean Water) for O and H, to V-PDB (Vienna Peedee Belemnite) for C and O, and to V-CDT (Vienna Cañon Diablo Troilite) for S.

Sandstones with carbonate cement were selected for cathodoluminescence study using a cold cathode instrument (CL8200mk3) coupled to a Nikon Labophot microscope with vacuum chamber on the stage at HyDrasa laboratories Université de Poitiers. Representative samples of altered rock from the Lajas Formation were selected to analyze textures and chemical compositions of clay minerals, carbonate and sulfides, using a JEOL® 5600 electron microscope equipped with a Bruker energy dispersive X-ray spectroscopy detector (EDX) at HyDrasa Poitiers and with Zeiss Evo MA15 microscope equipped with back scattered (BSC) and EDX detectors (Aztec Energy model) at Instituto de Investigación en Paleobiología y Geología (IIPG), Universidad Nacional de Río Negro-CONICET. Analytical conditions were accelerating voltage 15 kV, probe current 1 nA, working distance 17 mm, counting time of 60 s. The EDX analyses were calibrated using synthetic and natural oxides and silicates ($MnTiO_3$, hematite, albite, orthoclase, diopside, Cu and Mn) with corrections made using a ZAF program.

Sulfides from Barda González Deposits were analyzed for major and trace elements at the Universidad de Barcelona by an electron microprobe (Cameca SX-50) equipped with five wavelength dispersive spectrometers (WDS) and one energy dispersive spectrometer (EDS) silicon drift type detector (SDD) with 20.0 kV accelerating voltage, 10 nA beam current (standard mineral and material used were: chalcopyrite, Mn rhodonite, FeS_2, FeS, Mo, CdS, Sn, PbS, and Ag).

Metal assays of cuttings from the drilling were performed by Alex Stewart Laboratory (Assayers) Argentina S.A. at intervals of 1 m (Orión del Sur, 2008). The assay data were combined with the logging results from Orion del Sur S.A. to construct lithogeochemical cross sections. Rock samples from 10 drill cores of Cupen Mahuida hydrocarbon field were analyzed for 37 elements using energy dispersive X-ray fluorescence with an EDXRF Shimadzu 720 spectrometer at ATP Laboratorio S. R.L. The samples (crashed and homogenized) were ground to 30 mesh to avoid sampling uncertainties due to grain-size. The International standards used for these analyses included BHVO-1, SDC-1, MAG-1, SGR-1 and RGM-1.

4. Results

4.1. Ore mineralogy and geochemistry

4.1.1. Zn—Pb mineralization

At the Aguada Baguales oil field (Fig. 3A), Zn and Pb sulfides occupy the porosity of the coarse-grained facies of bed-load deposits irregularly distributed in the Lajas Formation, between 999.20 and 1007.11 m depth (Fig. 4A). The mineralization is hosted in the main oil reservoir layers of the Lajas Formation that show moderate and high content of light hydrocarbons yielding yellow fluorescence under UV. Manganese-rich siderite (MnO up to 10%) is interstitial to earlier marcasite (Fig. 6B) and is replaced by iron poor sphalerite (<1% Fe), patches of galena (Figs. 5, 7A–E), and traces of chalcopyrite. Sphalerite is the most abundant sulfide and occurs as yellow anhedral grains or, more common, as fibrous radial crystals around black spots of bitumen or marcasite (Fig. 7A–C, F–G). The fibrous radial habit supports a model of marcasite replacement by sphalerite. Late kaolinite and beidellite (Figs. 5, 6G) replace original illite and illite-smectite mixed layer silicates (Fig. 7H–I) and fill intergranular spaces.

At the Cupen Mahuida oil field (Fig. 3A), Zn and Pb mineralization is hosted in the coarsest facies (fluvial channel and distributary channel) of the Lajas Formation (Fig. 4B). Mineralization consists of fine to coarse grained iron-poor sphalerite, galena, and traces of chalcopyrite. Galena occurs as inclusions in coarse-grained sphalerite, interstitial or along the exfoliation of siderite crystals and disseminated with the illite, illite-smectite mixed layers cement. Zinc-Pb mineralization was also recognized at the base of the Huincul Formation (Figs. 3A, 4C) at the Cupen Mahuida oil field, between 420 and 430 m below the surface where it consists of yellow iron-poor sphalerite, galena and traces of chalcopyrite filling the remaining porosity of medium to coarse-grained sandstone.

4.1.1.1. Metal distribution. The highest zinc content (>1615 ppm) at Cupen Mahuida were recognized in 4 drill holes from 1700 to 2500 m depths (C-1, C-2, C-3, C-4; Figs. 3A, 4B, 8). Published seismic section shows that the location of these wells is coincident with the highest density of sub-vertical inverted rift faults (Coppo et al., 2018). The element concentration profiles for some of the studied wells show some correlations between Pb and As and between V and Ba. Most of the Zn anomalies coincide with Pb anomalies whereas Cu is only present in trace amounts. Similar metal contents were found at the top of the Los Molles Formation (well C-2; Fig. 8).

4.1.2. Cu mineralization

Copper mineralization is hosted in the middle section of the Huincul Formation (Fig. 4C) following an E-W trend at Tordillos and in the lower section of the Portezuelo Formation (Fig. 4C), whereas mineralized zones have a NE-SW trend at Barda González and NE-SW to N-S trends at La Cuprosa. Copper-bearing hypogene sulfides and supergene minerals occur disseminated in the main paleochannels, at the interface between bitumen and mudchips and, the contact between sandstone and silicified wood, filling fractures and shear zones (Fig. 9A–D). Copper minerals are

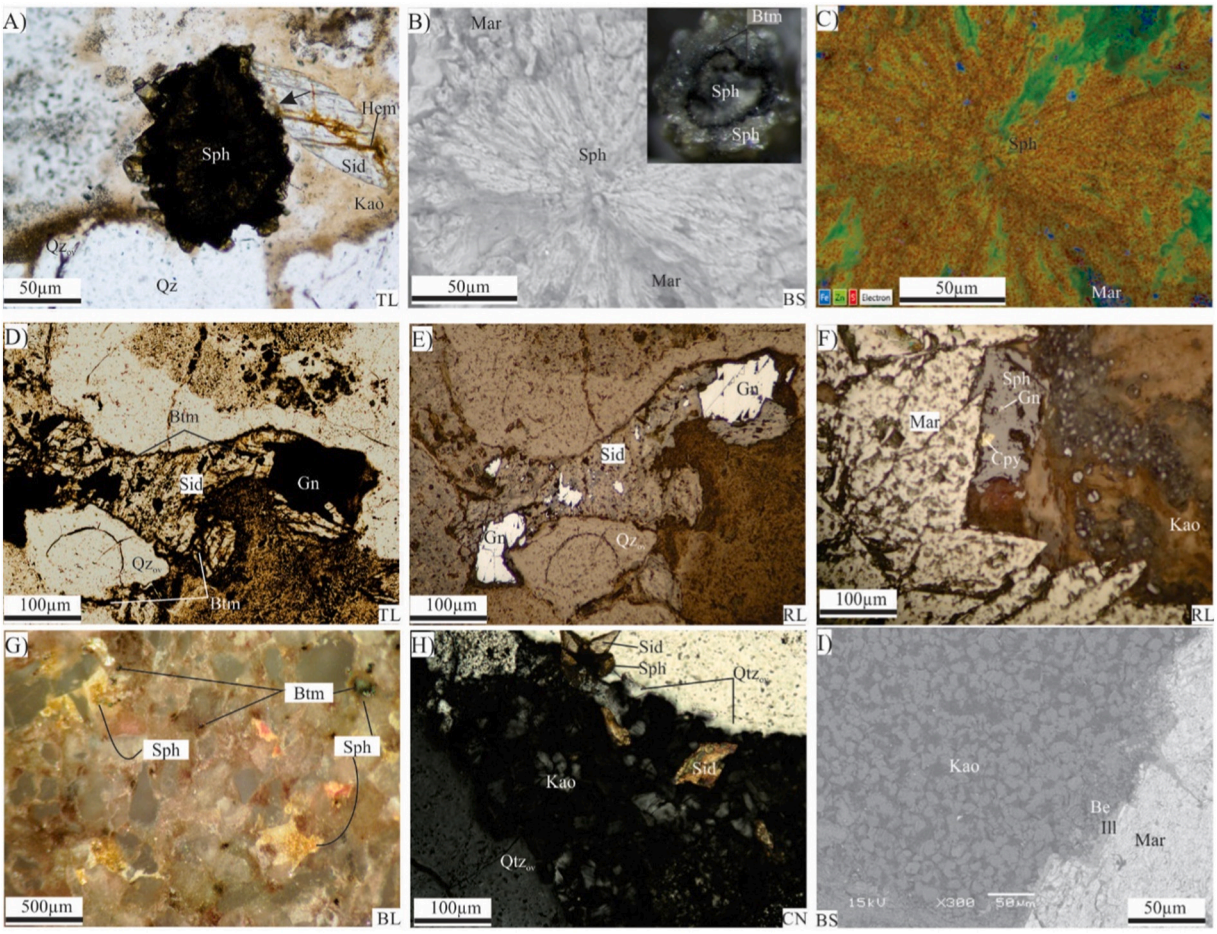

Fig. 7. Microphotographs of mineralized samples. A) Sphalerite, black arrow marks the siderite partially replaced by sphalerite. B) Backscattered electron microprobe image of the fibroradial-sphalerite, mesoscopic aspect in the upper right with concentric black bands formed by hydrocarbons inclusions. C) Sphalerite X ray elements map image show the lack of iron in sphalerite. D–E) Siderite partially replaced by galena. F) Sphalerite filling the porous spaces between marcasite, including tiny crystals of chalcopyrite and galena. G) Interstitial sphalerite and traces of bitumen in the sandstone. H) Siderite and sphalerite crystals, corroded quartz overgrowth and interstitial late kaolinite. I) Backscattered image shows book like habit of kaolinite crystals in transitional contact with beidellite, illite and marcasite. Type of images: BL: obtained with binocular loupe, BS: back scattered, CN: polarized microscope with transmitted light with crossed nicols, RL: with reflected light, TL: with transmitted light. Be: beidellite, Btm: bitumen, Cpy: chalcopyrite, Ill: illite, Gn: galena, Kao: kaolinite, Mar: marcasite, Mqz_{ov}: micro quartz Qz_{ov}: quartz overgrowth, Sid: siderite, Sph: sphalerite.

always in contact with bitumen, hence, in outcrops they show similar patterns described for bitumen (flames and tubes, Fig. 9E–H). In some places, bitumen is included or cut by Cu mineralization (Fig. 9I–J).

The deposits are affected by supergene alteration of the ore minerals, with sulfide abundance increasing with depth. Iron-Cu and Cu minerals (Fig. 5) occupy intergranular and intragranular porosity (Fig. 9K–M), detrital dissolution cavities and cleavage planes. They are also seen to replace detrital grains and previous cements, infill cracks and veinlets between 5 µm to a few mm width that cut both detrital grains and authigenic cements. These relationships support a late diagenetic origin for the mineralization; intense clast replacement results in oversized pores and floating texture (Fig. 9K–M). Mineralized flames and tubes at Tordillos (Fig. 9E) show a distinctive fracture pattern formed by sub horizontal anastomosing fractures that crosscut grains and diagenetic cements filled with sulfides, sulfates and supergene copper minerals (Fig. 9K). These flames and tubes contain: a) relicts of barite 1 coating, b) coarse crystals of barite 2 hosting abundant organic fluid inclusions and bitumen impregnations, and c) traces of pyrite. Barite 1, barite 2 and pyrite are partially to totally replaced by bornite, chalcopyrite and chalcocite group minerals (Fig. 9K–L), the later are the most widespread and abundant. Veinlets of barite 3 cut the sulfides and early cements. Relicts of Cu—Fe and Cu sulfides are only preserved as patches within the supergene minerals (Fig. 5) in the Portezuelo Formation at Barda González-La Cuprosa and consist of bornite and chalcocite-group minerals (Fig. 9M; Table A.1.). Traces of chalcopyrite fill micro fractures that cut grains and calcite cement, always at the contact with bitumen. SEM-EDS analyses detected UO (13.89–28.7%), CuO (3.54–30.45%), MnO (21.26–30.45%), and S (6.8–10%) anomalies on the bitumen surface.

In the studied deposits, several of Cu and V supergene minerals (Fig. 5) were recognized (covellite, malachite, brochantite, azurite, chrysocolla, tenorite, cuprite, possibly crednerite, volborthite, and atacamite) along with goethite, hematite and psilomelane. Covellite rims previous Cu—Fe sulfides and grades to brochantite (Fig. 9K–L), tenorite, and cuprite toward the contact with bitumen coating. Brochantite is one of the earliest supergene minerals that prevailed at Tordillos (Fig. 9K) whereas malachite and azurite are more abundant in the Barda González-La Cuprosa deposit (Fig. 9A–B, M). Efflorescence of volborthite and Ba-bearing volborthite in the bitumen surface occur in all deposits. At Tordillos, carnotite and francevillite fill the pore spaces between bitumen and barite 2 and coat bitumen (Fig. 9K). Chrysocolla is the latest and more widespread supergene mineral in all deposits (Fig. 9G, K). Close to the mineralized sandstone, the altered rocks show irregular iron oxide-rich halos cutting the sedimentary structures with relicts of pyrite (Fig. 9C).

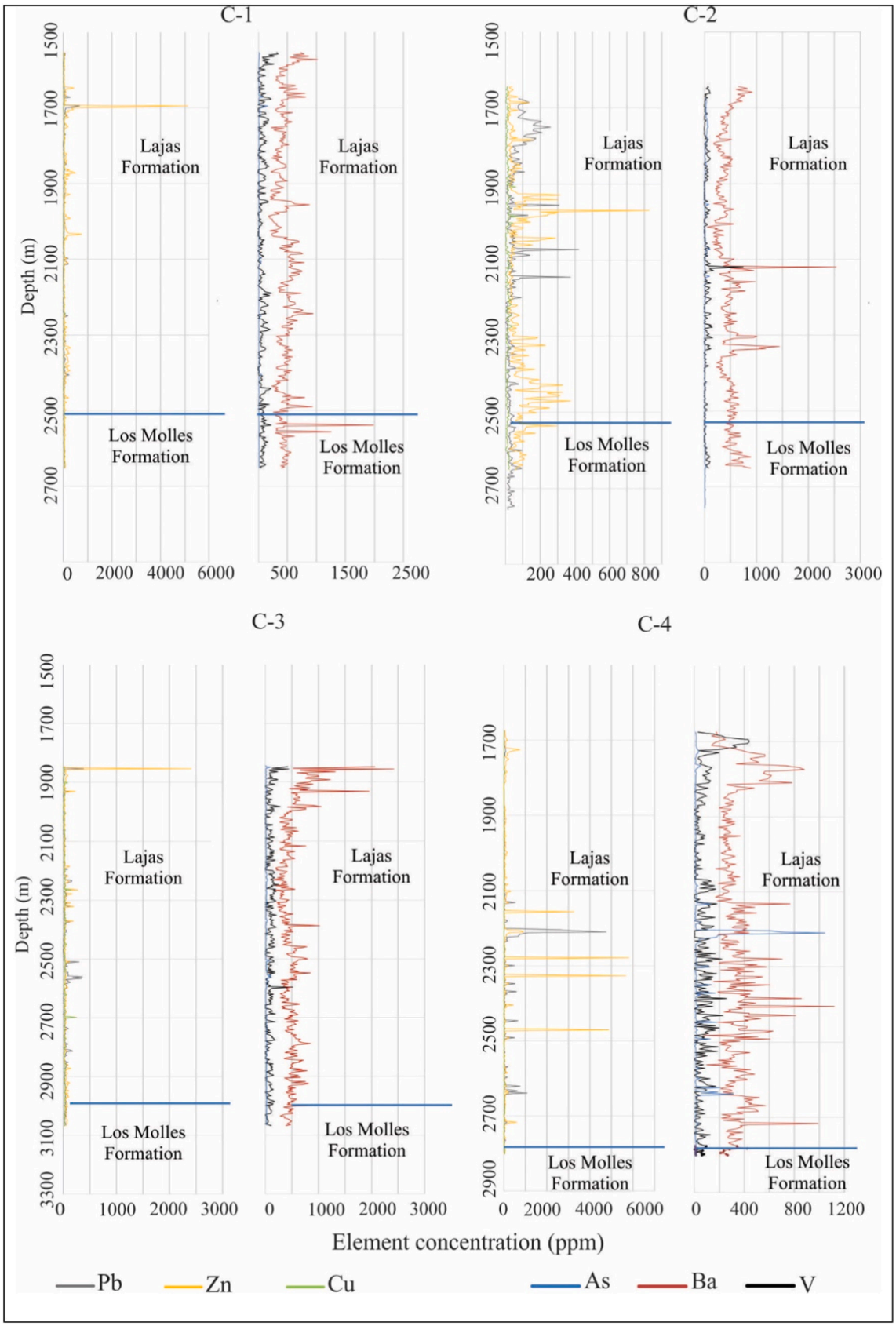

Fig. 8. Geochemical log profiles showing depth (m) versus element concentration (ppm) for different wells from the Cupen Mahuida hydrocarbon field. The blue line marks the boundary between the Lajas and the Los Molles formations. (For interpretation of the references to color in this figure legend, the reader is referred to the web version of this article.)

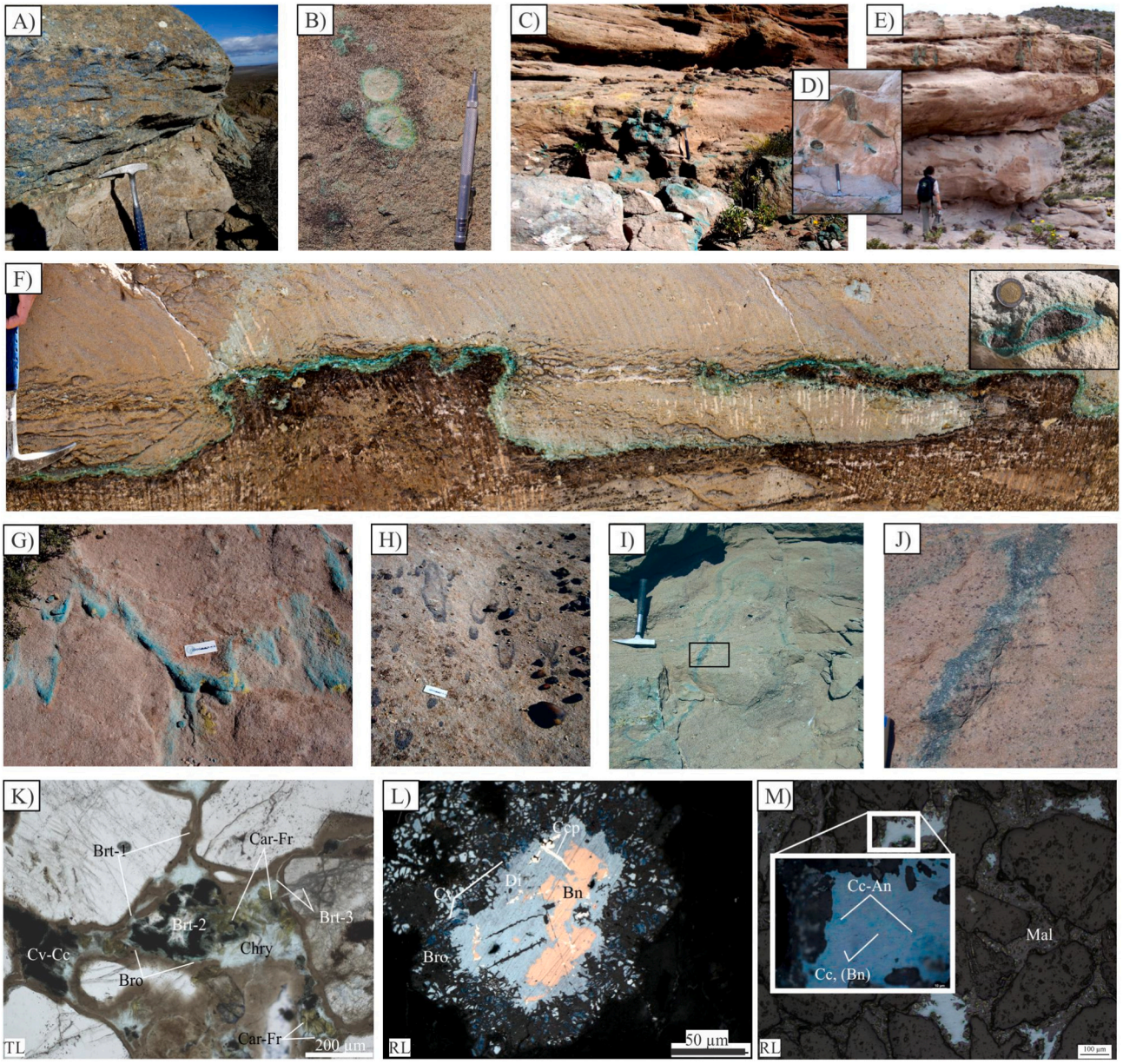

Fig. 9. A–M) Copper mineralization in sandstones of the Huincul and Portezuelo formations at Tordillos and Barda González-La Cuprosa deposits, respectively. K–M) Microphotographs of the representative green sandstone with hypogene and supergene copper mineralization and several generations of barite (see text for details). Bn: bornite, Brt1, 2, 3; barite1, 2, 3, Bro: brochantite, Btm: bitumen, Car: carnotite, Cc: chalcocite group minerals, Ccp: chalcopyrite, Chry: chrysocolla, Cv: covellite, Di: digenite, Fr: francevillite, Mal: malachite, TL: transmitted light, RL: reflected light. (For interpretation of the references to color in this figure legend, the reader is referred to the web version of this article.)

4.1.2.1. Metal distribution. At the Tordillos deposit major concentrations of Cu and V occur along the fluvial paleochannels of the Huincul Formation (Fig. 10). The highest V and Mn contents overlap with and extend below the zones with highest Cu grades (Fig. 10), corresponding to the location of the bitumen bearing sandstone. Erratic values of U (100–251 ppm) overlap with anomalous V (140–2090 ppm) and Cu (300–>10,000 ppm; Fig. 10; Pons et al., 2017) and correlate with the presence of U—V supergene minerals (e.g. carnotite and francevillite). Unaltered mudstone interbedded in the sandstone shows the highest Ba (321–2851 ppm) and Sr (115–629 ppm) values and the altered mudstone shows the highest Zn values (197–1251 ppm) (Fig. 10; Pons et al., 2017).

At the Barda González deposit, the highest Cu (>4000 ppm) and Mo (40 to 653 ppm) values are found in the most permeable facies (paleochannels) of the Portezuelo Formation. This reflects the presence of Cu sulfides with elevated Mo contents (Table A.1.). Copper anomalies coincide with Mn anomalies (100 to 3280 ppm, Fig. 11). The distribution of V overlaps the Cu-rich zones and the bitumen impregnations. There are Pb anomalies (500–1300 ppm) below the Cu-rich zones which correlate with Mo anomalies (Fig. 11). Zinc anomalies (204–691 ppm) occur in the altered mudstone interbedded in the bleached sandstone and reddish mudstone and generally have a positive correlation with Sr and Ba (Fig. 11).

4.2. Fluid inclusions petrography and microthermometry

Fluid inclusion (FI) microthermometry was carried out on quartz, calcite 3, calcite 4, barite 2 and analcime from the Tordillos and Barda González-La Cuprosa Cu deposits. No suitable fluid inclusions were found for analysis in either siderite or sphalerite with the Zn—Pb

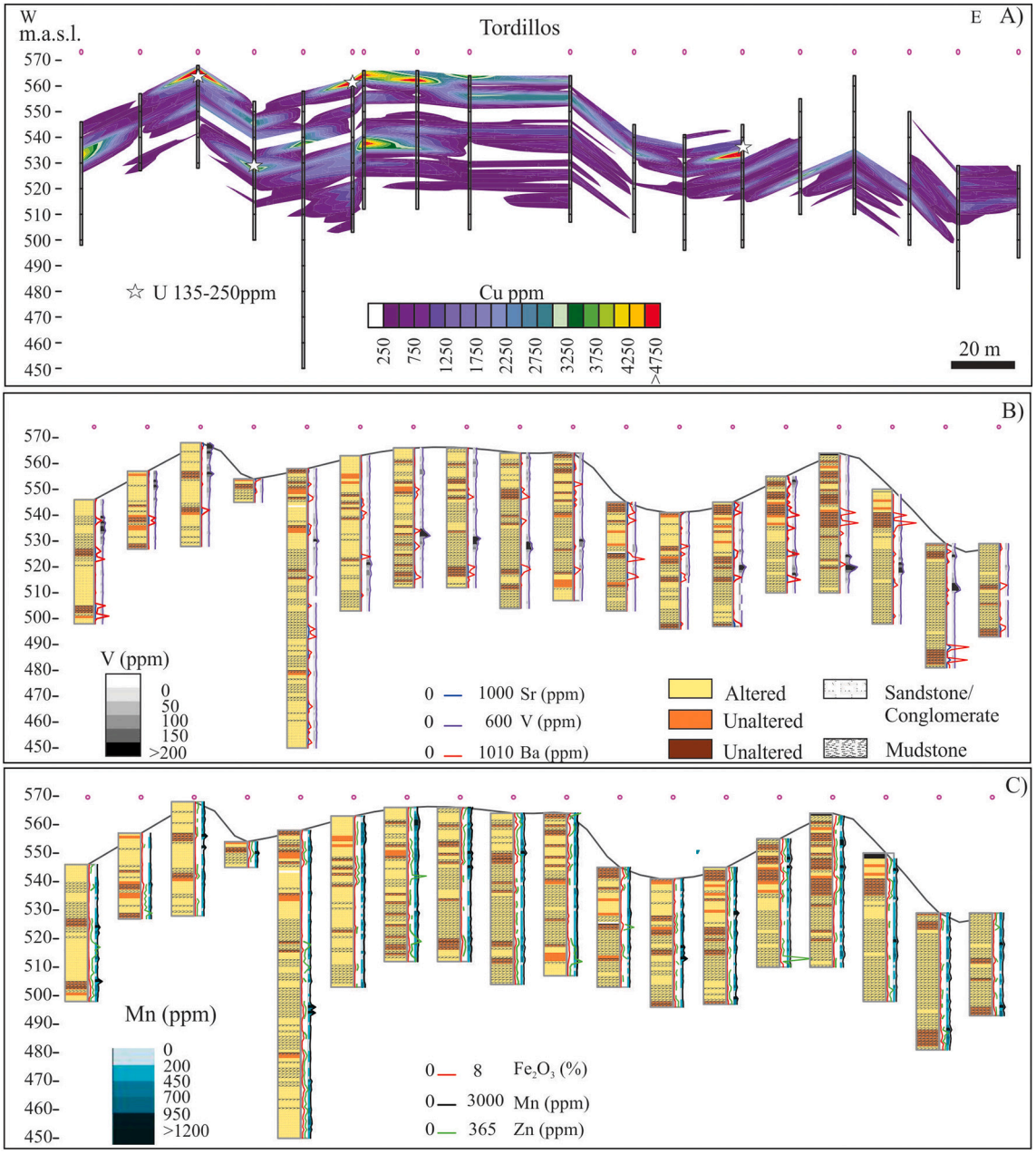

Fig. 10. West-east cross section along the main paleochannels of the Huincul Formation at the Tordillos deposit showing distribution of A) Cu, B) Sr, V, Ba, and C) Fe_2O_3, Mn and Zn. m.a.s.l.: meters above see level.

mineralization. Seven types of fluid inclusions were identified: Ia (L), Ib (L_o), IIa (L + B), IIb (L + B_o), IIc (L_o + B_o), IIIa (L_o + B_o + S) and IIIb (L + L_o + B_o) where I, II and III represent one, two- or three-phases fluid inclusions, respectively, and L is for aqueous liquid, L_o for hydrocarbons liquid, B for vapor bubble, B_o for hydrocarbon bubble and S for solid phase. The type Ia may represent metastable low temperature fluid inclusions with the same fluid than type IIa that failed to nucleate the bubble during cooling (Goldstein and Reynolds, 1994). Type IIc (L_o + B_o) fluid inclusions consist of two immiscible liquids, colorless and brown, with variable proportions of both liquids and the bubble shows adherence phenomena on the inclusion walls. Some organic phases in the fluid inclusions shows yellowish to green and blue fluorescence under UV. Fluid inclusion data are summarized in Table A.2A–B and Figs. 12, 13 and 14. Only primary and pseudo secondary fluid inclusions were analyzed in diagenetic minerals. Regular to irregular secondary fluid inclusions, 2.5 to 160 μm in size, aligned with either pyrite or bitumen were studied in sealed fractures of detrital quartz.

4.2.1. *Tordillos deposit*

Quartz overgrowths host primary (Fig. 12A–B) and pseudo-secondary fluid inclusions of co-genetic types Ia, IIa, and organic rich types Ib, IIb, and IIIb. These inclusions occur parallel or perpendicular to the growth zone and are cogenetic with pyrite (Fig. 12A). Similar fluid inclusion assemblages were identified in sealed fractures of quartz that also cut the micro-quartz overgrowth. Along the same trend of fractures there are hydrocarbon impregnations in contact with anhedral pyrite.

Type IIa fluid inclusions in quartz overgrowth homogenize to liquid between 91.5 °C and 120 °C (n = 22; Fig. 13A). First melting temperature range from −35 °C to −9.5 °C (n = 11) indicating the presence of dissolved NaCl-$MgCl_2$, $FeCl_2$ and KCl (Borisenko, 1977). Final ice melting temperatures range from −7 °C and − 0.5 °C (n = 14), with corresponding salinities between 1.5 and 10 wt% NaCl equiv. (Goldstein

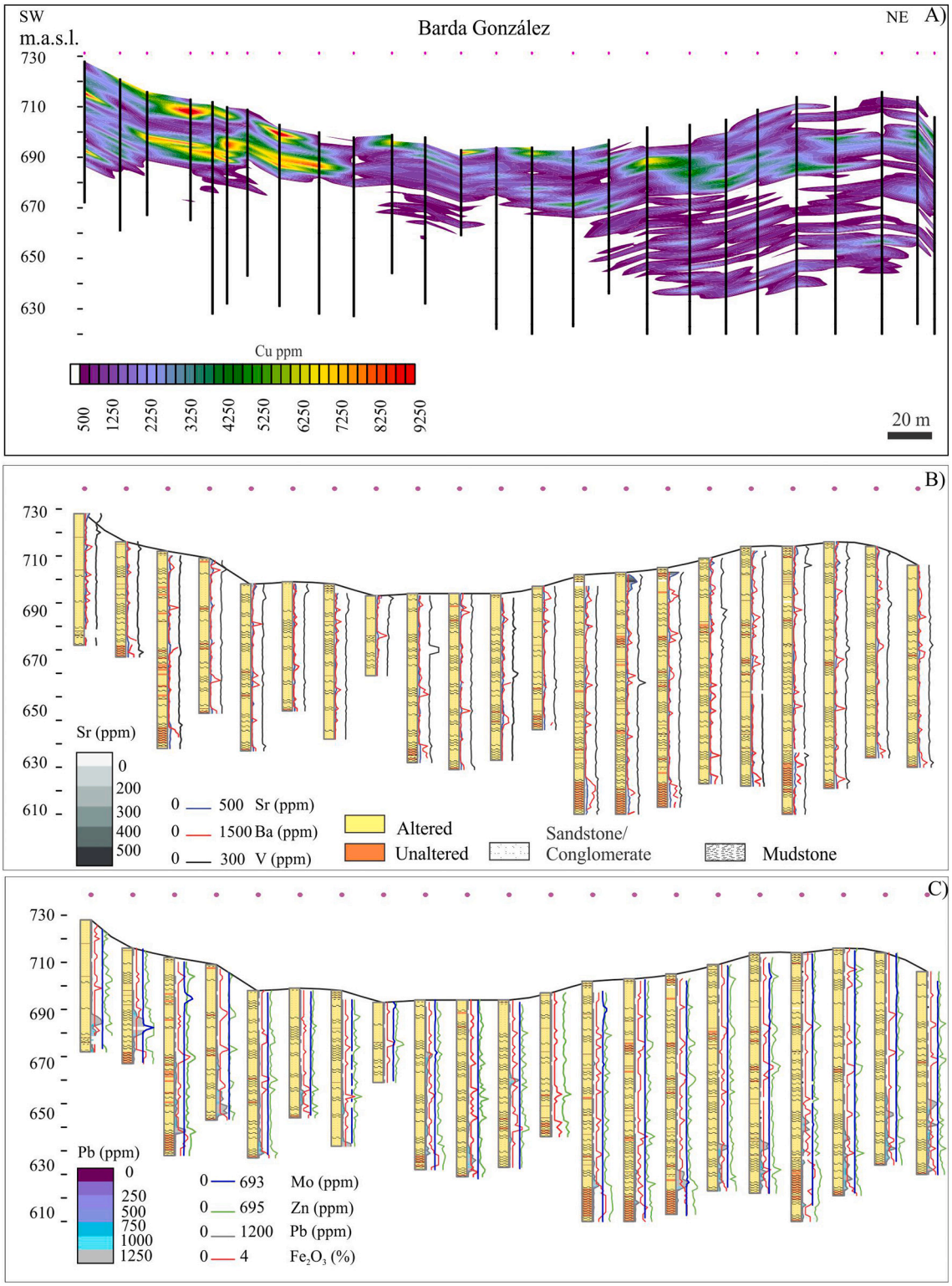

Fig. 11. Northeast-southwest cross section through the main paleochannels of the Portezuelo Formation at the Barda González deposit showing distribution of A) Cu, B) Sr, Ba, V, and C) Mo, Zn, Pb and Fe_2O_3. m.a.s.l.: meters above see level.

and Reynolds, 1994, Table A.2A). Type IIb fluid inclusions in quartz overgrowth homogenize to liquid at 104 °C (n = 2) or did not homogenize before to 150 °C (n = 1; Fig. 13A). First melting temperature of the liquid phase separated from the bubble range from −151 °C and −60 °C and for the liquid phase between −29 °C and − 6 °C (n = 2). They show clathrate final melting temperature from +6 °C to +21 °C (n = 4). Similar behavior was observed in type IIb fluid inclusions hosted in sealed quartz fractures (Table A.2A). Clathrate formation indicates the presence of carbonic species (Collins, 1979), which, together with blue fluorescence of the liquid phase, also confirm the presence of hydrocarbons. Type IIa fluid inclusions along sealed fractures yield homogenization temperatures from 96 °C to 146 °C (n = 7).

Barite 2 crystals in contact with chalcocite group minerals have greenish to orange fluorescence and host abundant triangular, regular

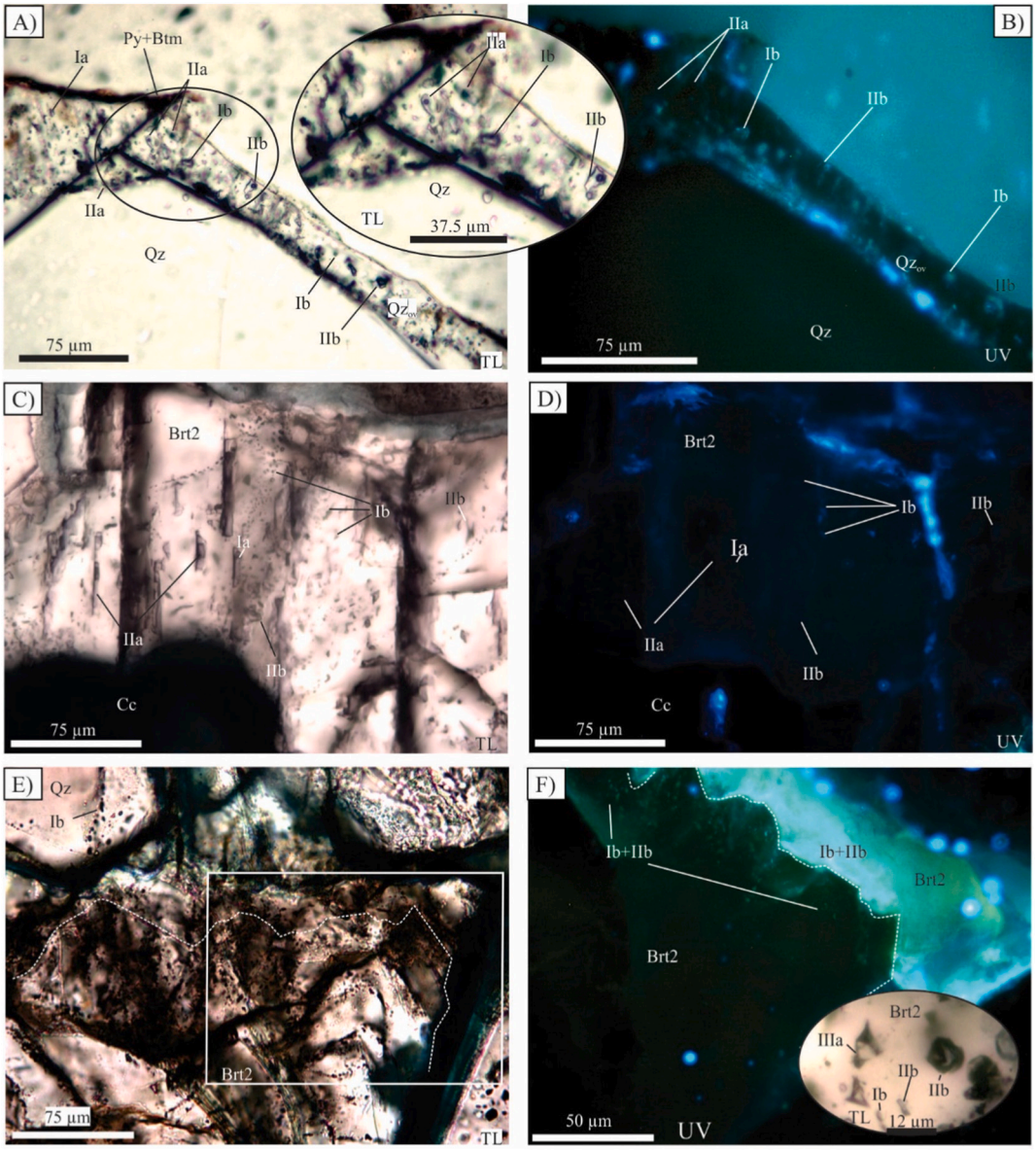

Fig. 12. A–F) Microphotographs of fluid inclusions hosted in diagenetic minerals from the Huincul Formation (see text for explanation). Brt2; barite 2, Cc: chalcocite, Qz; quartz, Qz_{ov}: quartz overgrowth, TL: transmitted light, UV: ultraviolet light.

and irregular fluid inclusions of type Ia, IIa, Ib, IIb, IIIb, and IIIa (Fig. 12C–F). Some of the type IIIa fluid inclusions contain an unidentified greenish daughter crystal (Fig. 12F). Primary types Ib, IIa and IIb fluid inclusions form trends parallel to both cleavage planes (Fig. 12C–D) and growth zones. Pseudo secondary fluid inclusions are distributed in a radial pattern that converge in the chalcocite crystals (Fig. 12C–D). Type Ib fluid inclusions are the most abundant and show a greenish yellow fluorescence (Fig. 12E–F). Type IIb fluid inclusions contain a liquid showing greenish yellow to blue UV fluorescence and a non-fluorescent bubble. Type IIa fluid inclusions in barite homogenize to liquid between 95 °C and 101 °C (n = 3) and the contemporaneous type IIb fluid inclusions homogenize to liquid at 119 °C (n = 2; Fig. 13A, Table A.2A). Type IIb fluid inclusions show clathrate final melting at +0.8 °C (n = 2).

Calcite 3 and calcite 4 host numerous fluid inclusions like those observed in barite 2, quartz overgrowth and quartz sealed fractures. Most are types Ib fluid inclusions, less common are type IIb associated with non-fluorescent tiny type IIa fluid inclusions, while type IIIb fluid inclusions are scarce (Fig. 14A–B; Table A.2A). Organic-rich fluid inclusions (types Ib, IIb and IIIb) show green yellowish to blue fluorescence (Fig. 14B, D; Table A.2A). Type IIa fluid inclusions in calcite 3 and 4 homogenize to liquid between 100 °C and 170 °C (n = 14; Fig. 13A). Type IIb fluid inclusions homogenize to liquid at 117 °C (n = 1) and other type IIb do not homogenize above to 120 °C (n = 7). Bubbles of types IIb and IIIb fluid inclusions deformed after cooling between −145 °C and −180 °C and recovered their original appearance at temperatures between −81 °C and −60 °C (n = 4), typical behavior of inclusions containing organic fluids (Burrus, 1981). First melting temperatures of the aqueous phase are between −37 °C and − 21 °C for type IIb (n = 4) and from −46 °C to −14 °C for type IIIb (n = 2), indicative of the presence of chlorides with monovalent and divalent cations (Borisenko, 1977). These inclusions show clathrate final melting temperature from +7 °C to +19.6 °C (n = 6; Table A.2A).

4.2.2. *Barda González deposit*

Calcite 2 rims developed on calcite 1 and clastic grains, coarse-grained calcite 3 and calcite 4 (Fig. 14E–H) host numerous fluid inclusions. Calcite 3 and calcite 4 show a zonation marked by the

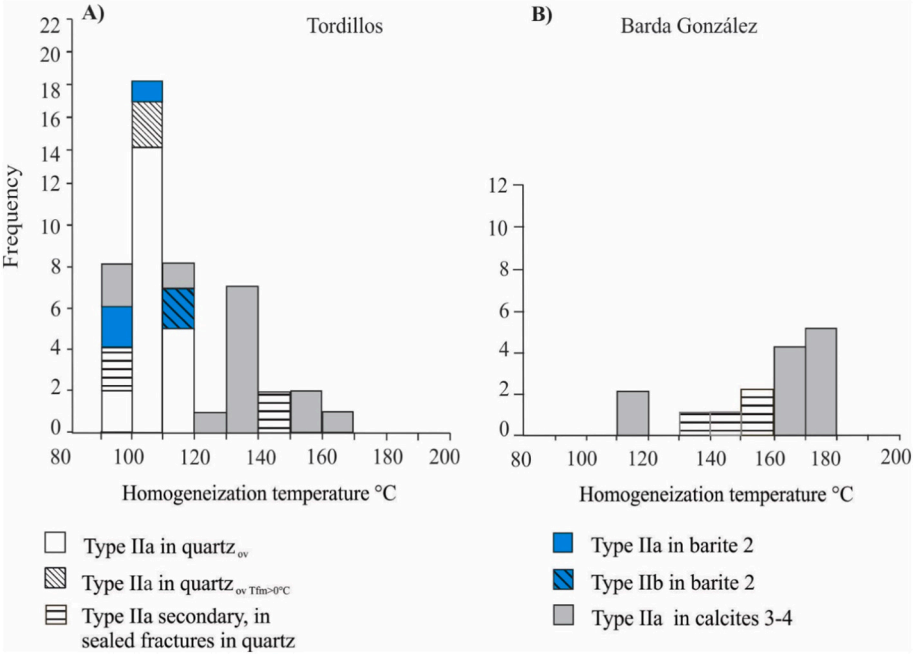

Fig. 13. Homogenization temperatures (Th) of fluid inclusions hosted in diagenetic minerals from the A) Huincul Formation at the Tordillos deposit and B) Portezuelo Formation at the Barda González deposit. Tfm: ice final melting temperature.

alternation of inclusion bands with greyish-green UV fluorescence that host primary fluid inclusions (<2–12.5 μm) and non-fluorescence bands (Fig. 14E). Calcite 3 and the cloudy calcite 4 host numerous fluid inclusions with the following characteristics: (1) regular (triangular shape), one-phase fluid inclusions (types Ia, Ib), (2) irregular to regular, two-phase fluid inclusions (types IIa, IIb, IIc), and (3) irregular multiphase fluid inclusions (IIIb). All fluid inclusions types are associated with tiny euhedral pyrite crystals.

Type Ib fluid inclusions show a yellowish green UV fluorescence when occurring in the calcite 3 crystals and a light-blue fluorescence when hosted in calcite 4 (Fig. 14E). Most type IIa are very small (3 μm), non-fluorescent liquid-rich fluid inclusions showing low relief and a tiny pink bubble (Fig. 14F–H). Type IIb and IIc fluid inclusions present a variable liquid:bubble ratio (70:30 and 60:40), a yellowish-green fluorescence, low-relief liquid, and non-fluorescent high-relief bubble. The three-phase fluid inclusions show variable behavior under UV light, but frequently the liquid phase shows green to light-blue fluorescence (Fig. 14E; Table A.2B). Quartz grains host trends of secondary fluid inclusions in healed fractures along with bitumen and pyrite, similar to the fluid inclusions described for calcite 3 and calcite 4 (Table A.2B). Type IIa fluid inclusions hosted in healed fractures in quartz homogenize to liquid at temperatures from 134 to 160 °C (n = 5). (Fig. 13B; Table A.2B). Type IIa fluid inclusions hosted in calcite 3 homogenize to liquid at ranges of 113–115 °C (n = 2) and 170–185 °C (n = 5; Fig. 13B; Table A.2B). Salinity measurements could not be performed because of decrepitation during cooling.

4.3. Stable isotope geochemistry

4.3.1. Oxygen and hydrogen isotopes

δD and $\delta^{18}O$ isotopic composition of smectite and chlorite + chlorite-smectite mixed layer clays was determined from the bleached sandstone facies of the Huincul Formation at Tordillos. The δD and $\delta^{18}O$ isotopic composition of smectite varies from −92.4‰ to −87.5‰ and +17.4‰ to +18.4‰ respectively (Fig. 15, Table 1). The δD and $\delta^{18}O$ values of chlorite + chlorite-smectite mixed layers are −82.8‰ to −85.2‰ and +16.2‰ to +18.3‰, respectively. The δD and $\delta^{18}O$ isotopic compositions of current formation water from the Lajas Formation are −37.5‰ and −4.65‰, respectively (Fig. 15, Table 1).

4.3.2. Carbon and oxygen isotopes

The $\delta^{13}C$ and $\delta^{18}O$ isotopic composition of several calcite generations and $\delta^{13}C$ of bitumen from the Tordillos and Barda González deposits are shown in Table 2 and Fig. 16. Calcites 1, 2, 3 and 4 from the bleached sandstone at Tordillos have $\delta^{13}C$ from −11.5‰ to −5.6‰ and of $\delta^{18}O_{SMOW}$ from +14.6 to +22.8‰ (n = 13). The highest $\delta^{13}C$ and $\delta^{18}O$ values correspond to samples with early diagenetic calcite 1 partially replaced by calcite 3 and 4. The lowest values of $\delta^{13}C$ (from −10.1‰ to −11.9‰) belong to samples dominated by calcite 4 which show similar isotopic composition to bitumen impregnations (−10.3‰, n = 1; Fig. 16).

The $\delta^{13}C$ and $\delta^{18}O$ values of calcites (calcite 2, 3, 4 and 5) from the Barda González deposit vary from −0.3‰ to −12.3‰ and from +20.8‰ to +26.5‰, respectively (n = 10; Fig. 16, Table 2). The highest values are from the late calcite 5 (late caliche) and the lowest values correspond to calcite 3 and calcite 4 partially replaced by malachite. Bitumen shows $\delta^{13}C$ values between −24.4‰ and −15.9‰ (n = 3; Fig. 16, Table 2). The $\delta^{18}O$ of fluids in equilibrium with calcites at Tordillos and Barda González-La Cuprosa were calculated using range of homogenization temperatures (100–170 °C and 113–185 °C, respectively) obtained from aqueous fluid inclusions and the fractionation of O'Neil et al. (1969). The $\delta^{18}O$ of fluids in equilibrium with calcite 3 and calcite 4 from the Tordillos deposit were from +0.4‰ to +8.2‰ and from −2.5‰ to +7.6‰, respectively. The $\delta^{18}O$ of fluids in equilibrium with calcites (2 to 5) from Barda González-La Cuprosa were from +5‰ to +16.1‰.

4.3.3. Sulfur isotopes

The results of S isotope analyses from sulfides hosted in the Lajas and Huincul formations at Aguada Baguales and Cupen Mahuida and from sulfides and sulfates at Tordillos and Barda González-La Cuprosa are shown in Table 3 and Fig. 17. Pyrite hosted at Lajas Formation from the Cupen Mahuida oilfield displays the widest range of $\delta^{34}S$ values from −11.6‰ to +18.1‰ (n = 3). Marcasite at the Aguada Baguales oilfield shows $\delta^{34}S$ values between −3.5‰ and −2.2‰. Galena shows a $\delta^{34}S$ value of 5.2‰ (n = 1) and sphalerite has heavier and homogenous $\delta^{34}S$ values between +10.4‰ and +10.8‰ (n = 3). The equilibrium isotopic

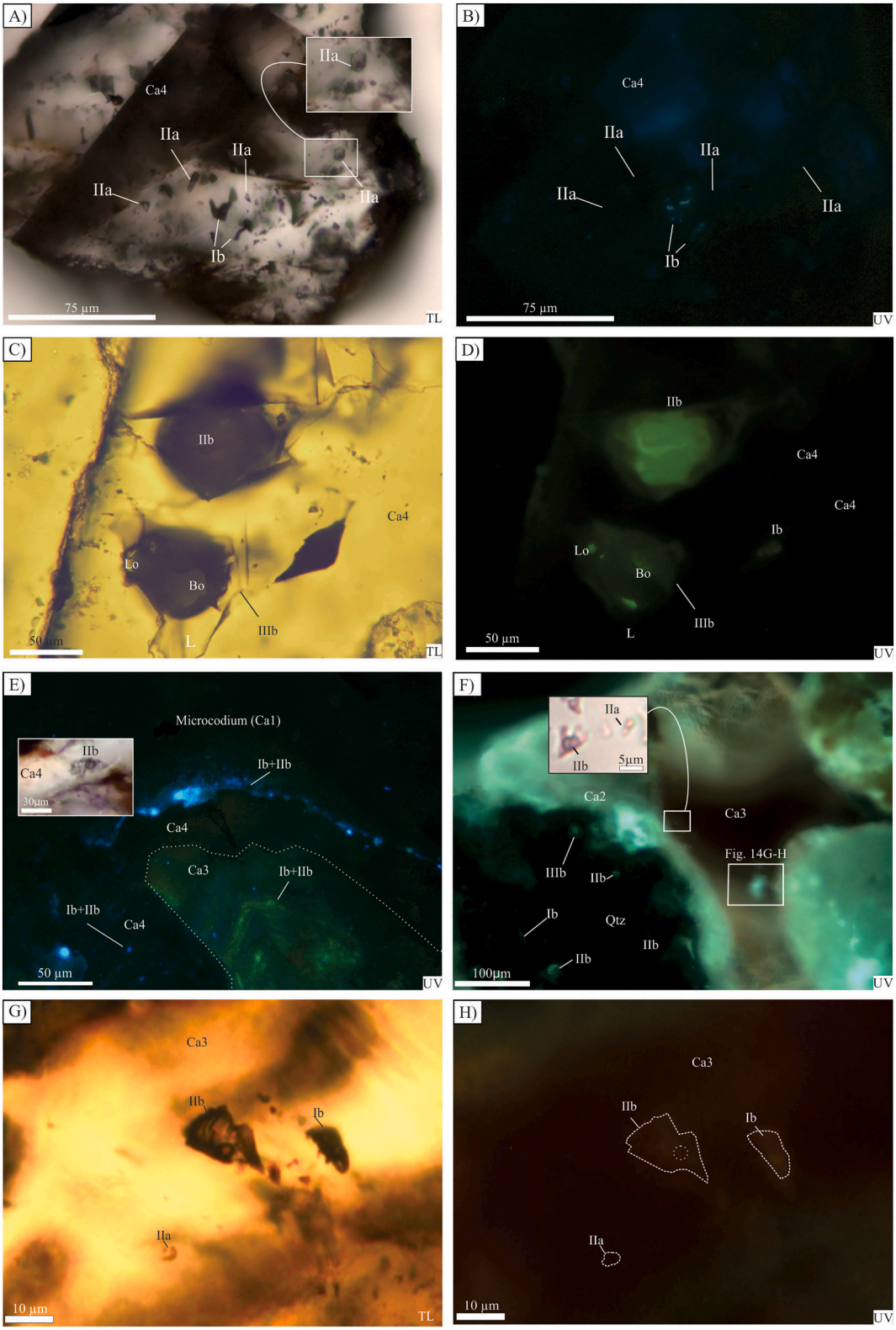

Fig. 14. Microphotographs of fluid inclusions hosted in diagenetic calcite from the A–D) Huincul and E–H) Portezuelo formations (see text for explanation). Ca: calcite, Qz: quartz; TL: transmitted light, UV: ultraviolet light.

temperature range calculated for the sphalerite-galena pair is 119 and 123 °C using the equations of Kiyosu (1973) and Liu et al. (2015), respectively. Framboidal pyrite and sphalerite hosted in the sandstone of the Huincul Formation at Cupen Mahuida oil field have $\delta^{34}S$ of −8.3‰ and +8.3‰, respectively.

The chalcocite group minerals at Tordillos have $\delta^{34}S$ values from −18.7‰ to −7.8‰ (n = 13) with a highest frequency between −18.7‰ and −15.0‰ (n = 8) (Table 3; Fig. 17). The less negative values correspond to sulfides containing relicts of barite. This was confirmed with the duplication of an analyses of hand-picking sulfide which shows $\delta^{34}S$

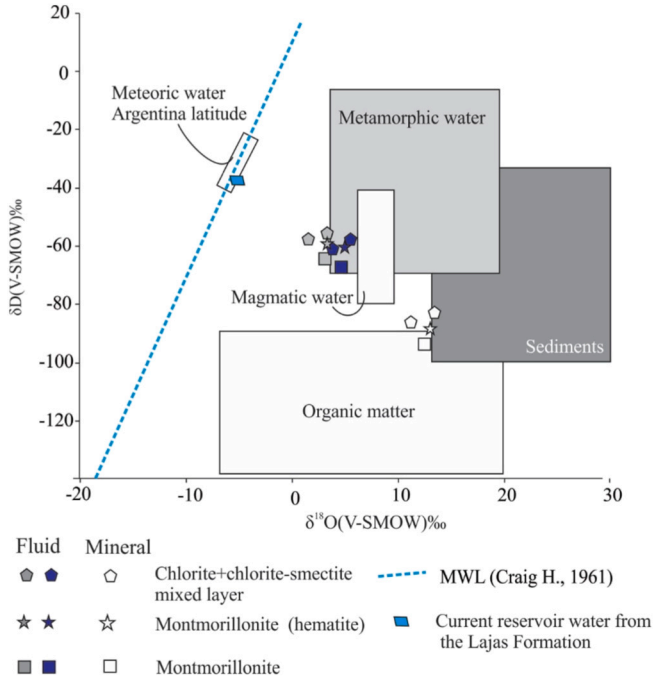

Fig. 15. Plots of δD versus $\delta^{18}O$ of clay minerals (in white) and of fluids in equilibrium with clay minerals from the Tordillos deposit (in gray and blue color, calculated for minimum and maximum temperatures, respectively; after Sheppard, 1986; see text form explanation). The are represented the meteoric water line and the isotopic composition of meteoric water at Argentina, which has not been substantially changed since the Tertiary (Yurtsever and Gat, 1981). (For interpretation of the references to color in this figure legend, the reader is referred to the web version of this article.)

values higher (−7.8‰) than sulfides separated by chemical extraction (−15.3 to −15.9‰; Table 3). A crystal of barite 2 displays $\delta^{34}S$ values of −5.9‰. At Barda González, chalcocite group minerals have $\delta^{34}S$ from –21.3‰ to −18.9‰, with an outlier of −0.9‰. Late gypsum shows a $\delta^{34}S$ value of −3.0‰ (Table 3; Fig. 17).

5. Discussion

5.1. Alteration of the Mesozoic siliciclastic host rocks

At the Aguada Baguales and Cupen Mahuida hydrocarbon fields (Figs. 1, 3A), the coarsest facies of the Lajas Formation behaved as conventional and unconventional reservoir rocks, respectively (Raggio et al., 2014) (Fig. 4A, 18A). The earliest diagenetic minerals identified in the sandstone of the Lajas Formation are gypsum-anhydrite, followed by quartz overgrowth formed during compaction and burial (Fig. 18B). Quartz overgrowth in the Lajas Formation started to precipitate after the Los Molles Formation reached the hydrocarbon generation window (160–140 Ma, Late Jurassic to Early Cretaceous, Veiga, 2002). Increasing burial of the Lajas Formation resulted in a reduction of porosity from 25% to <17% (Cruz et al., 2002; Veiga, 2002).

The main vertical expulsion of hydrocarbons from the source rocks (Los Molles Formation) to the Lajas Formation at Aguada Baguales and Cupen Mahuida anticlines (Fig. 3A) took place during Neocomian times (Early Cretaceous, Veiga, 2002; Fig. 18A). However, some oil-gas lateral migration at Aguada Baguales from the north of the basin cannot ruled out, where the Vaca Muerta Formation reached the oil maturation window (Cruz et al., 2002; Villar et al., 2005). Hydrocarbon migration was accompanied by 10 times as much formation water (Surdam et al., 1989). The current reservoir fluids in the oil-gas field (formation waters) from the main reservoir rocks located north of the Huincul High (Lajas, Lotena and Mulichinco formations; Figs. 2, 3) have salinities range between 26 and 160 g/l NaCl equiv. consisting mainly of chlorides with $CO_3^{=}$, CO_3H^-, $SO_4^{=}$ H_2S and Na^+, Ca^{2+}, K^+, Mg^{2+}, Sr^{2+}, Mn^{2+}, and Ba^{2+}

Table 2
Carbon and oxygen isotopic data from the Tordillos and Barda González deposits.

Sample number	Description	Luminescence	$\delta^{13}C_{PDB}$	$\delta^{18}O_{PDB}$	$\delta^{18}O_{SMOW}$
Tordillos					
To 140209-4	Ca 1 cut by Ca 4	Cal 1, n.l.; Cal 4 orange	−5.6	−7.9	+22.81
To 21107-8 Cc	Ca 3 with spots of Ca 4	Cal 3 red; Cal 4 orange	−9.7	−13.0	+17.54
To 21107-11	Ca 3, interstitial Ca 4	Cal 3 and 4 orange	−7.1	−10.5	+20.11
To 21107-12 Cc	Ca 3	Orange to yellow	−9.5	−13.0	+17.51
To140209-17Ca1	Ca 4 > 2 (external zone)	Orange	−9.5	−13.0	+17.49
To 140209-17ca-2	Ca 2 > 4 (core)	Orange	−7.7	−11.1	+19.45
To 11108-5-3	Ca 2 and 4	n.a.	−10.7	−11.9	+18.6
To 11108-6-3-1	Ca 2 and 4 (core)	Red to orange	−9.6	−13.4	+17.08
To 11108-6-3-2	Ca 2 and 4 (external zone)	Red to orange	−9.7	−12.0	+18.6
To 070209-14	Ca 4	Orange	−11.4	−15.8	+14.59
To 111209-6A-C	Ca 4	Orange	−11.5	−13.5	+17
To 111209-6A	Ca 4	Orange	−11.9	−13.1	+17.41
To 21107-3 Cc	Ca 4	Orange	−10.1	−13.6	+16.88
To 11108-6-1	Bitumen		−10.3		
Barda González					
BG 300807–8-1*	Ca 3 + 4	Dull	−8.1	−9.8	+20.85
BG 300807–8-2*	Ca 4	Red to orange	−8.5	−9.8	+20.77
BG 300807–8-3*	Ca 5	Non-luminescence	−4.9	−7.7	+22.95
BG-100	Ca 5	n.a.	−0.3	−4.3	+26.49
BG 1-Ca	Ca 3	n.a.	−4.9	−8.1	+22.61
BGDes-1-12	Ca 2 + 3	n.a.	−7.0	−4.4	+26.33
BGDES-1-3	Ca 2 + 3	Red	−7.5	−9.0	+21.67
BG10*	Ca 4 + Mal	Red	−12.4	−7.7	+22.97
Dan-1	Ca 2	n.a.	−7.7	−8.3	+22.33
Dan-2	Ca 3	n.a.	−8.1	−8.7	+21.98
BGDes-1-12BTM	Bitumen	n.a.	−22.4		
BG1-btm	Bitumen	n.a.	−24.4		
BG110510–13	Bitumen	n.a.	−15.9		

All the data have been analyzed at the Servicio de Isótopos Estables, Universidad de Salamanca. Cal: calcite; Mal: malachite; Py: pyrite.
* Isotope analyses from Pons et al., 2015.

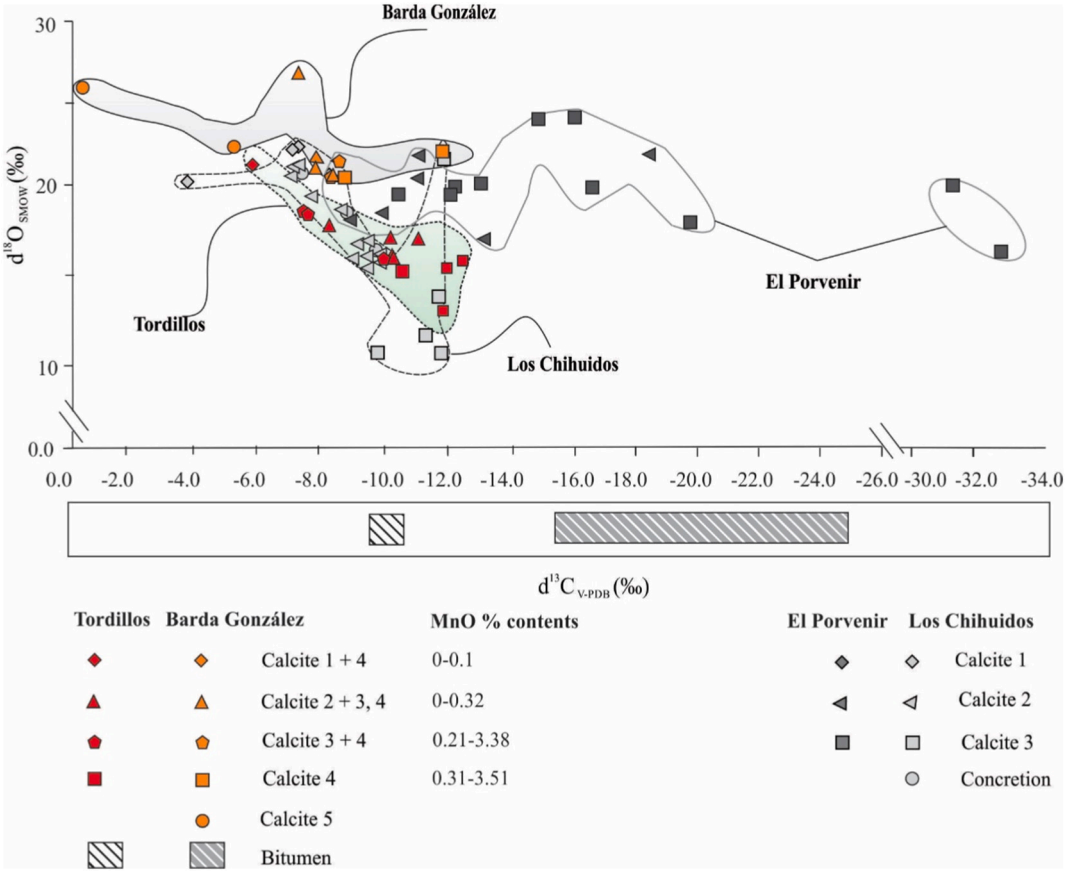

Fig. 16. Plots of $\delta^{13}C$ versus $\delta^{18}O$ of calcite 1 to 5 and $\delta^{13}C$ range of bitumen from the Huincul and Portezuelo formations in the SHCD of the Neuquén Basin. The isotopic composition of calcites from other Cu deposits located south of the Huincul High (El Porvenir) and at Los Chichuidos High (Los Chihuidos; Rainoldi et al., 2019) are shown for comparison.

as soluble cations (Vottero and González, 2002; Malone et al., 2002; Schiuma et al., 2002; Pons et al., 2009; Pons et al., 2015). These formation waters could have formed by the expulsion of the interstitial connate water and/or dissolution of evaporites from the Mesozoic sequence of the basin (Figs. 2, 18A). Their temperature was likely to reach between 79 °C to 170 °C (~1700 to ~3500 m) base on the total burial depths of the Lajas Formation reconstructing the now eroded sedimentary rocks above the Neuquén Group (~700 to ~1000 m; Pons et al., 2015; Pons et al., 2017), and clearly represents a normal geothermal gradient (Sigismondi and Ramos, 2009).

Marcasite and pyrite ± illite (illite-smectite mixed layers) formed after quartz overgrowth in the presence of liquid hydrocarbons based on the presence of bitumen between quartz and marcasite ± clays (Fig. 18B). The S isotopic composition of marcasite at Aguada Baguales (−2.2‰ and −3.5‰; Fig. 17) is depleted by 19.5 to 22.0‰ relative to sulfate from evaporite formations in the Neuquén Basin ($\delta^{34}S$ +17.3‰ to +18.5‰; Lo Forte et al., 2005), which reflects the sulfur isotopic composition of Jurassic seawater. Considering this isotopic fractionation and a temperature of 80 °C for the total burial depth (~1800 m depth) of the Lajas Formation at Aguada Baguales (Sigismondi and Ramos, 2009), marcasite could have precipitated via bacterial sulfate reduction (BSR; $1000\ln\alpha SO_4\text{-}H_2S$ > 20‰, T: <80 °C; Machel, 2001). The presence of marcasite indicates fluids having a pH < 5 (Murowchick and Barnes, 1986). The sulfur isotopic composition of pyrite (+18.1 to −11.6‰; Fig. 17) at Cupen Mahuida oil field is depleted by 0.4‰ to 30.1‰ relative to sulfate from evaporite formations ($\delta^{34}S$ +17.3 to +18.5‰; Lo Forte et al., 2005) and could likely be formed by BSR of aqueous sulfate in a closed system from less acidic fluids (pH > 5; Murowchick and Barnes, 1986) than fluids from the Aguada Baguales oil field.

During, Tertiary Andean tectonism (Cruz et al., 2002; Mosquera and Ramos, 2006; Silvestro and Zubiri, 2008) earlier faults were reactivated in the Huincul High, triggering a number of phases of hydrocarbon migration directly from source or reservoir rocks (Vottero and González, 2002, Malone et al., 2002) into to the Huincul and Portezuelo formations (Fig. 3; Fig. 18A). The regional bleaching of the Huincul and Portezuelo sandstone layers impregnated with bitumen, are strong evidence of secondary oil migration into these zones (Pons et al., 2015; Rainoldi et al., 2015; Paz et al., 2016; Pons et al., 2017; Rainoldi et al., 2019). Furthermore, quartz (micro and meso) overgrowth, barite 2 and calcite 2–4 from the bleached sandstones (Fig. 18C) all contain primary hydrocarbon-bearing fluid inclusions. This regional alteration is concentrated mainly in the Huincul and Portezuelo formations because other formations of the Neuquén Group (Candeleros and fine-grained mudstone of Cerro Lisandro and Plotier formations; Fig. 4B) behaved as sealed rock. In the coarse-grained facies of the Candeleros Formation analcime and carbonate cements reduced the porosity to <3.5% of the total rock volume (Quarisa, 2017; Rainoldi et al., 2019).

The influx of hydrocarbons and brine into the red bed resulted in dissolution of hematite coatings with reduction of Fe^{3+} to Fe^{2+} which combined with reactive sulfate to precipitate pyrite and marcasite. The range of sulfur isotope composition obtained for marcasite ($\delta^{34}S$ −36.4 to +18.2‰) and pyrite ($\delta^{34}S$ −60.2‰ to −24‰; Fig. 17) located at the base of the Portezuelo Formation at the Barda González-La Cuprosa deposits (Fig. 4B), suggest that biogenic sulfate reduction (BSR) occurred in a gradually closed system with respect to sulfate for marcasite, whilst in an open system with unlimited sulfur source for pyrite at temperatures <100 °C (Seal, 2006).

The δD and $\delta^{18}O$ isotopic compositions of clay minerals from the

Table 3
Sulfur isotopic data of sulfides and sulfates from Tordillos, Barda González deposits and from Aguada Baguales and Cupen Mahuida occurrences.

Zone	Sample	Mineral	Formation	$\delta^{34}S_{V\text{-}CDT}$
Aguada Baguales	AB1-T14a	Sph	Lajas	+10.4
	AB1-T11	Sph	Lajas	+10.8
	AB1-T5	Sph	Lajas	+10.8
	AB1-T14b	Ga	Lajas	+5.2
	AB1-T10	Marc	Lajas	−2.2
	AB1-T5	Marc	Lajas	−3.5
Cupen Mahuida	C-21700***,[1]	Py	Lajas	+18.1
	C-21762[1]	Py	Lajas	+3.4
	C-21712[1]	Py	Lajas	−11.6
	C-3420[1]	Sph	Neuquén Group	−8.3
	C-3420[1]	Fram-Py	Neuquén Group	+8.3
Tordillos	To-21107-6-l***,[1]	Cc-Cv	Huincul	−10.1
	To-21107-6	Cc-Cv	Huincul	−17.5
	To-21107-17-l	Cc-Cv	Huincul	−18.703
	To-21107-17-l***[1]	Cc-Cv	Huincul	−11.7
	To 270410-15**	Cc-Cv	Huincul	−15.9
	To 270410-15-2	Cc-Cv	Huincul	−7.8
	To-121110-1B**	Cc-Cv	Huincul	−7.3
	To-270410-6**	Cc-Cv	Huincul	−17.3
	To-270410-6	Cc	Huincul	−17.7
	To-270510-14	Cc-Cv	Huincul	−15.4
	To 270410-15-l**	Cc-Cv	Huincul	−15.273
	To 2110714-B	Cc-Cv	Huincul	−15.2
	To2110714-B	Brt2	Huincul	−5.9
	To 270410-6	Cc-Cv	Huincul	−17.2
Barda González	BG 43624*	Marc	Portezuelo	−24.4
	BG 43920*	Py	Portezuelo	−60.2
	BG 46325*	Py	Portezuelo	−59.8
	BG 4325*	Py	Portezuelo	−36.4
	BG 43624*	Marc	Portezuelo	+18.2
	BG 110510-12**	Cc-Cv	Portezuelo	−0.9
	BG 110510-2c	Cc-Cv	Portezuelo	−18.9
	BG-300807-10A	Cc-Cv	Portezuelo	−21.2
	BG-300807-9A	Cc-Cv	Portezuelo	−21.3
	BG1-Cc-Cv	Cc-Cv	Portezuelo	−20.9
	BG 150911-5	Gy	Portezuelo	−3

Brt2: Barite 2; Cc: Chalcocite group minerals; Cv; covellite; Fram-Py: framboidal pyrite; Ga: galena; Gy: gypsum; Mar: marcasite; n.a.: not analyzed; Py: pyrite; Sph: sphalerite.

* Isotope analyses from Pons et al., 2015; samples analyzed at the Servicio de Isótopos Estables, Universidad de Salamanca.

** Sample separation methods by chemichal extraction.

*** Sample analyzed by in situ Laser ablation analyeses.

[1] Indicate samples analyzed at Scottish Universities Environmental Research Centre.

Tordillos deposit lie on the boundary of sedimentary and organic matter fields (Fig. 15). The partial transformation of montmorillonite into chlorite and chlorite-smectite mixed layers yielded an additional source of silica, leading to the precipitation of micro-quartz overgrowths (Mosser-Ruck et al., 2010), probably at temperatures ~100 °C (Robinson and Santana de Zamora, 1999). The isotopic composition of fluids in equilibrium with montmorillonite and chlorite + chlorite-smectite mixed layers were calculated from temperature range of aqueous fluid inclusions hosted in cogenetic quartz overgrowth (91.5–120 °C), using the equations of Yeh (1980) for hydrogen and Sheppard and Gilg (1996) for oxygen, since there are no equations applicable to mixed-layer minerals and consistent with the presence of V-bearing specular hematite along the redox front in equilibrium with montmorillonite (~100 °C; Pons et al., 2017, Sugimoto et al., 1996; Catling and Moore, 2003). Oxygen ($\delta^{18}O_{fluid}$ of +1.1 to +6‰) and H (δD_{fluid} −67.5 to −55.3‰) isotope compositions of fluids in equilibrium with clay coatings are heavier and lighter, respectively, than the local meteoric water ($\delta^{18}O$ from −6‰ to −4‰, δD from −38‰ to −22‰; Sheppard, 1986 modified from Yurtsever and Gat, 1981) and plot close to the metamorphic fluids field (Fig. 15). Considering the absence of metamorphic rocks in the region, the isotope compositions of fluids in equilibrium with clay coatings may have resulted from the interaction of formation water with brines + hydrocarbons (Faure, 1986; Sheppard and Gilg, 1996). The lighter δD signature with respect to Cenozoic meteoric water confirm that carboxylic acids derived from hydrocarbons were involved in the genesis of these clay coatings (Pons et al., 2017; Rainoldi et al., 2014; Fig. 15).

Quartz overgrowth also precipitated from heterogeneous fluids (hydrocarbons + brines) at temperatures between 91.5 and 120 °C and salinities between 1.5% and 10 wt% NaCl equiv. (Fig. 13). First melting temperatures of fluid inclusions in quartz overgrowth (−35 °C and −9 °C) indicate the presence of $FeCl_2$ or NaCl–$MgCl_2$ (n = 4) and KCl (n = 10), respectively. This wide salinity range may indicate the mixing of interstitial water with the incoming brine that migrated with hydrocarbons. Barite 2 precipitated from similar heterogeneous fluids (hydrocarbon + brines) close to the feeder zones (Pons et al., 2017) at temperatures of 95–119 °C (Fig. 13). The sulfur isotopic composition of barite 2 (−5.9‰; Fig. 17) is consistent with the involvement of S derived from hydrocarbons of the source rocks (e.g. Vaca Muerta Formation contains sulfur-rich type IIS kerogen south of Huincul High; Villar et al., 2005). Considering that Ba could be transported as $BaCl_2$ in reduced acidic brines and given that barite is only weakly soluble under oxidized sulfate-stable conditions (Lydon, 1983), the increase in the oxygen fugacity of reduced brines + hydrocarbons as fluids met the red beds may have resulted in barite 2 precipitation (Cooke et al., 2000). This is consistent with the distribution of Ba anomalies close to the feeder fluid zones at the Tordillos deposit (Pons et al., 2017).

The multistage calcite cements are more widespread than barite in the sandstones of the Huincul and Portezuelo formations at the Tordillos and Barda González-La Cuprosa deposits, respectively, and precipitated from heterogeneous fluid systems (hydrocarbons + brines + interstitial water) at minimum entrapment temperatures of 100–185 °C (Fig. 13). This wide range of temperatures is consistent with the temperatures obtained from primary and secondary aqueous fluid inclusions in quartz overgrowth and quartz sealed fractures, respectively (96.5–146 °C at Tordillos and 134–160 °C at Barda González-La Cuprosa; Fig. 13). Therefore, this temperature range could represent multistage of hot hydrocarbon + brine upflow, as suggested by different fluorescence colors of fluid inclusion (yellow to blue). The light carbon isotopic signature of multistage calcite cements at Tordillos (−12.3‰ to −7.0‰) is similar to the $\delta^{13}C$ of calcite 2–4 from the Barda González-La Cuprosa deposits (−12.4‰ to −4.9‰; Table 2, Fig. 16), compatible with a similar C source. Calcite 4 shows the most negative values of $\delta^{13}C$, like the composition of the associated bitumen (−24.4‰ to −10.3‰; Table 2, Fig. 16). The wide range of $\delta^{13}C$ in calcite 2 to 4 may represent different mixtures of organic carbon (Machel et al., 1995) from the oxidation of hydrocarbons from Los Molles and Vaca Muerta source rocks (−9.6‰ and −57.1‰, respectively; Ostera et al., 2016) with remobilized carbon sourced from the dissolution of calcite 1 precipitated during the early diagenesis (−5.6‰; Fig. 16). A common byproduct of the redox reaction in this system is the iron sulfide precipitation (Machel et al., 1995) represented by tiny euhedral pyrite crystals associated with organic fluids inclusion hosted in calcite 3 and 4. A similar isotopic trend was observed in multistage calcite cements in other sediment hosted Cu deposits of the basin (Rainoldi et al., 2019) (Fig. 16). The MnO content (0 to 3.51%) increases as $\delta^{13}C$ and $\delta^{18}O$ decreases from calcite 1 to calcite 3 and 4 (Fig. 16). The incorporation of Mn in calcite 2, 3 and 4 is indicative of reducing condition during its precipitation (Pons et al., 2015, 2017). Higher $\delta^{18}O$ values of fluids in equilibrium with calcites from Barda González-La Cuprosa deposits than fluids from the Tordillos deposit (Figs. 3, 4B) can be explained by 1) a major degree of hydrocarbon biodegradation that could cause and increase of $\delta^{18}O$ in the residual oxygen (Pradeep et al., 1997) or 2) the involvement of brines with higher $\delta^{18}O$ coming from deepest zones of the basin during their formation (Kesler et al., 1997).

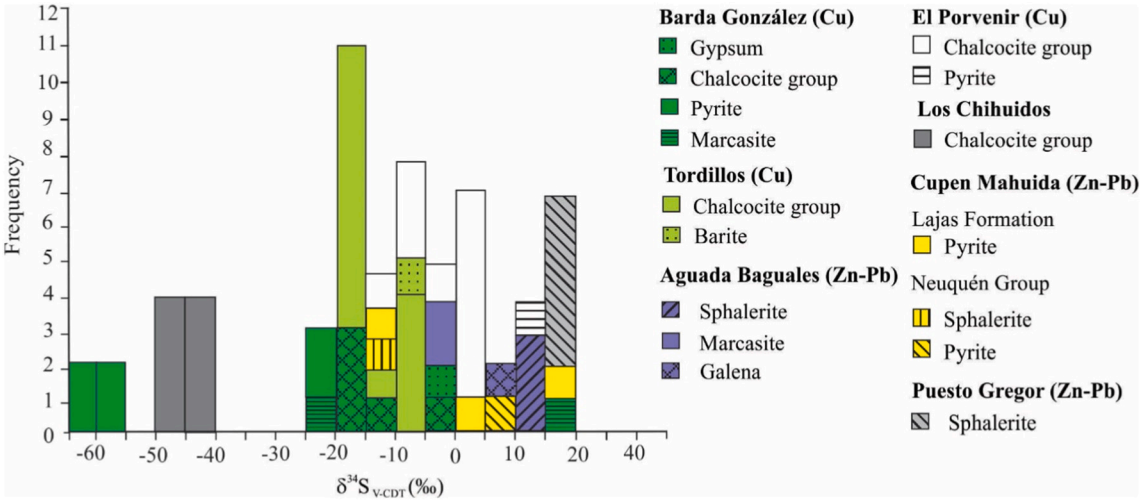

Fig. 17. $\delta^{34}S$ data from sulfides and sulfate hosted in the Lajas Formation (Cupen Mahuida and Aguada Baguales oil fields) and in the Huincuil and Portezuelo formations (Tordillos and Barda González-La Cuprosa deposits, respectively). $\delta^{34}S$ data of sulfides hosted in the Lajas Formation at Puesto Gregor (Garrido et al., 2000) and in the Huincul Formation at El Porvenir and Los Chihuidos High (Rainoldi et al., 2019) are shown for comparison.

The multiple trends of fluid inclusions (organic + aqueous; Table A.2) hosted in detrital quartz and feldspar grains were trapped during the reaction of organic acid with previous minerals that caused fluctuations of pH (from >8 to <8) and CO_2 fugacity (Pons et al., 2015). The abundance of organic-rich fluid inclusions suggests that during the formation of the alteration minerals the hydrocarbon to aqueous fluids ratio was high. The variable fluorescence color of these organic fluid inclusions (Figs. 12B, D, F, 14B, D–F) indicates the presence of hydrocarbons with different compositions (variable API gravity, Riecker, 1962; George et al., 2001). These different compositions could be caused by (1) fluctuation of the groundwater table in the reservoir that resulted in different extents of biodegradation (more intense at the oil water contact) or (2) different hydrocarbon pulses having a different evolutionary history (England et al., 1987; Larter et al., 2006).

5.2. Mineralization stage

During subsequent tectonic stages (Eocene, Middle to Late Miocene, Mosquera and Ramos, 2006; Rodríguez et al., 2007; Zamora Valcarce et al., 2006) the reactivation of the structures at basin scale may have promoted renewed up flow of Zn—Pb and Cu charged basinal brines into the siliciclastic Mesozoic rocks (Fig. 18A). There is a clear correlation between the distribution of metals anomalies with the main subsurface structures and oil fields (Fig. 3) at the Huincul High. Zinc and Pb anomalies are mainly hosted in the Lajas Formation (minor in the Huincul Formation) and associated with one of the main reactivated N-S rift structures (Coppo et al., 2018). Copper mineralization is hosted in the bleached red beds of the Neuquén Group associated with subsurface structures (Pons et al., 2017; Fig. 3). It is clear that mineralizing fluids could follows the same migration paths used by hydrocarbons at Aguada Baguales, Cupen Mahuida, Ricón del Mangrullo (close to the Tordillos deposit) and Barda González hydrocarbon fields (Schiuma et al., 2002, Pons et al., 2015; Paz et al., 2016; Pons et al., 2017; Coppo et al., 2018; Figs. 3, 18A). Basinal brines could have evolved from the reservoir water via basin scale convective migration to a higher oxidation state by reaction with the underneath evaporite successions of the Embayment (e.g. Tábanos, Auquilco, Huitrín and Rayoso formations; Figs. 2, 3). Thus, the most likely S source for Zn, Pb, Fe—Cu and Cu sulfides is the sedimentary sulfur carried by the brines from the dissolution of evaporites (see also El Desouky et al., 2010) as was determined by Rainoldi et al. (2019) for Los Chihuidos and El Porvenir stratiform copper deposits from the Neuquén Basin. This hypothesis is also supported by the scarcity of sulfate and iron sulfides in the host rocks (i.e. sulfides absent in the red beds and only minor to traces in the bleached rocks) and the lack of a possible magmatic S source in the studied areas.

Basinal brines were able to leach Zn and Pb from the rocks underlying the Lajas Formation. Zinc (220–400 ppm), Pb (100 ppm), and V (250 ppm) anomalies observed in the Los Molles Formation at Cupén Mahuida oil field (Fig. 8) and also in another oil field located to the east, in the Huincul High (Ostera et al., 2016), suggest that these black shales may have supplied Zn and Pb during the circulation of basinal fluids (Fig. 18A). Basinal brines could have leached Cu from the thick red beds (Tordillos Formation, Bajada del Agrio Group, and Neuquén Group; Figs. 2A, 3, 18A) underlying the Huincul and Portezuelo formations. At the Paradox Basin, (Colorado, USA) for similar style deposits Hahn and Thorson (2006) describe the convection of warm (70–110 °C) brines (50–200 g/l NaCl equiv.) as the main fluids capable to leach and transport Cu from the red beds. Considering that the solubility and precipitation conditions of Cu, Zn, and Pb are similar in low temperature systems like these (Haynes and Bloom, 1987), we speculate that different pulses of metal-charged basinal brines may have been involved in the Zn—Pb and Cu mineralization hosted in the Lajas Formation (Huincul Formation) and the Neuquén Group, respectively.

At the Aguada Baguales oilfield (Fig. 3A) textural evidence indicates that Pb—Zn sulfides and siderite precipitated after marcasite, pyrite ± illite (illite-smectite mixed layers) cements because of the input of oxidized basinal brines ($SO_4 > H_2S$), capable of transporting Pb and Zn (Cooke et al., 2000). At the Cupen Mahuida oil field, the same well crosscut similar Zn—Pb mineralization at different depths and lithologies (at ~1850 m depth in the Lajas Formation and at 450 m depth in the Neuquén Group well C-3; Figs. 3A). Paleocene to Miocene Andean tectonism is likely to have caused the connection of the Lajas reservoir rocks with the Neuquén Group by the reactivation of previous faults (Schiuma et al., 2002; Mosquera and Ramos, 2006). The interaction of these oxidized fluids with hydrocarbons hosted in the sandstone probably resulted in the precipitation of Zn—Pb sulfides due to the change in oxygen fugacity of fluids in the presence of hydrocarbons. Siderite could precipitate as by-product of this redox reaction at temperatures <150 °C within a pH range of 5 to 7 (Cooke et al., 2000). The sulfur isotope composition of sphalerite (+10.4 to +10.8‰) and galena (+5.2‰) are depleted by 6.5 to 13.3‰ relative to evaporite sulfate ($\delta^{34}S$ +17.3‰ to +18.5‰; Lo Forte et al., 2005). The temperature estimated from the isotopic composition of the sphalerite-galena pair (119–123 °C; Kiyosu, 1973 and Liu et al., 2015, respectively) is consistent with the temperature obtained from fluid inclusions hosted in dolomite associated with Zn—Pb sulfides in the Lajas Formation outcrops at Puesto Gregor

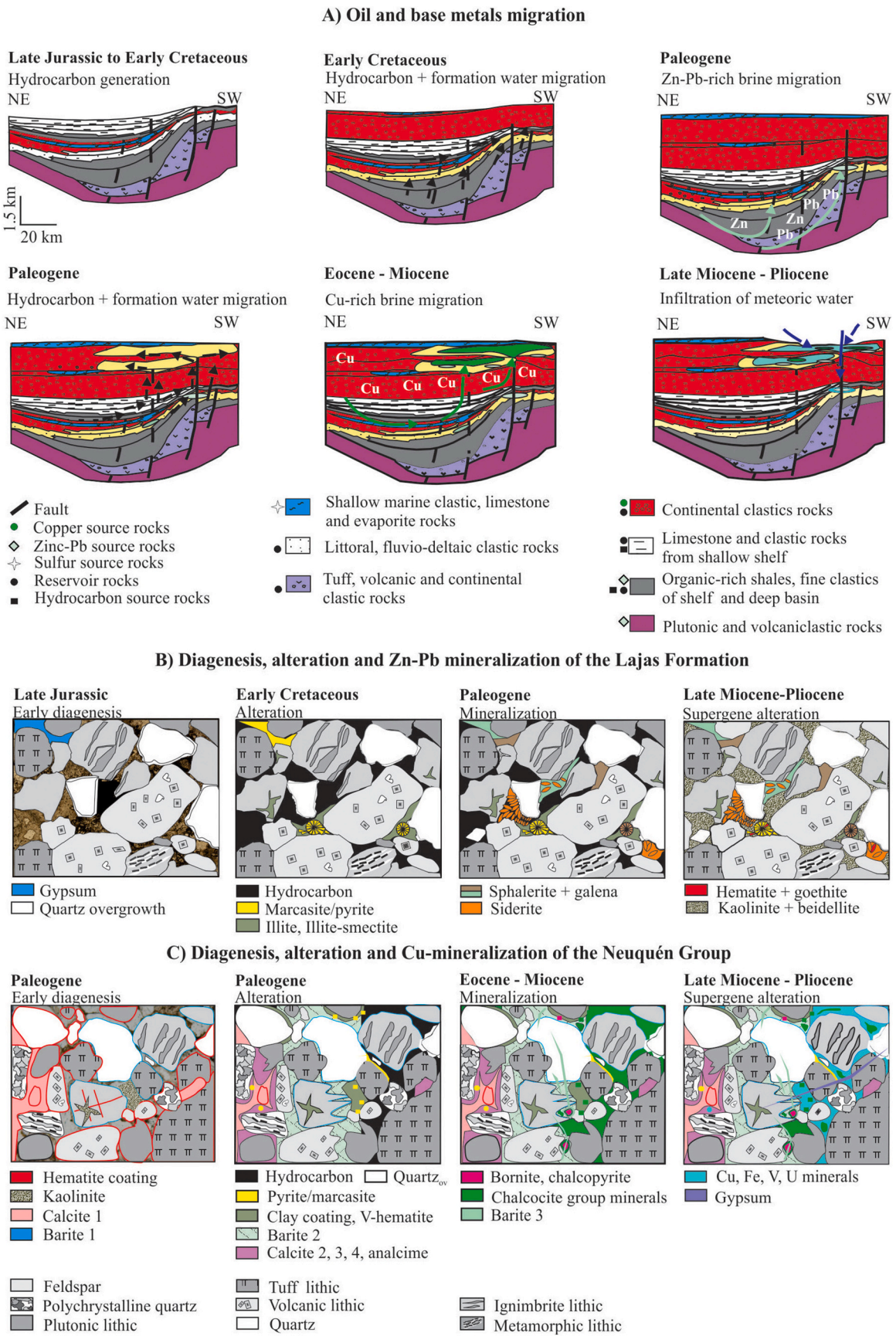

Fig. 18. A) Schematic diagram showing the evolution of the Neuquén Basin (cross section located in Fig. 1A (modified from Cruz et al., 2002) and the fluid migration stages, B) the concomitant diagenetic, alteration and mineralization stages of sandstones from the Lajas Formation and C) from the Neuquén Group in the Huincul High region.

(140 °C, Cesaretti et al., 2002) (Fig. 1A). The small $\delta^{34}S$ shift in addition to the assumed formation temperature of sulfides (>100 °C) indicate they precipitated by TSR at a higher temperature than marcasite (Orr, 1977, Machel, 1987, 1989). The sphalerite hosted in the base of the Huincul Formation at Cupen Mahuida has a $\delta^{34}S$ value of −8.3‰ (n = 1; Fig. 17), depleted by 23.3‰ relative to sulfate in evaporite units ($\delta^{34}S$ 17.3–18.5‰; Lo Forte et al., 2005). This is larger isotope fractionation than sphalerite hosted in the Lajas Formation at Aguada Baguales.

At Tordillos and Barda González-La Cuprosa, the irregular distribution of Fe—Cu and Cu sulfides in the Huincul and Portezuelo formations could be explained by the tortuous fluid migration and interconnection of channels through the frontal lobe of fluvial facies (lateral migration between channels) and erosive surfaces (vertical migration while the flooded facies constituted barriers to the passage of fluids (Paz et al., 2016). Copper mineralization is hosted in altered paleochannels of the Hunicul and Portezuelo formations, and its spatial association with bitumen at macro- and micro-scale indicates that Cu-rich fluids entered the paleochannels when they were reduced and acting as oil reservoirs or carrier beds (Pons et al., 2009; Pons et al., 2017). The local feeder zones for these brines seem to have been the vertical tubes and fractures (Fig. 9C–E).

The partial dissolution and replacement of barite 1 and barite 2 by bornite-chalcopyrite at the Tordillos deposit could have occurred by sulfate reacting with warm chloride brines (>100 °C) also carrying Cu (Hanor, 2000). Coeval bornite and chalcopyrite implies a temperature of formation above 100 °C (Haynes and Bloom, 1987). This temperature falls into the highest solubility range for barium sulfate and subsequent temperature decrease could cause Ba saturation and precipitation of barite 3 (Hanor, 2000). The predominance of chalcocite with wide laterally distribution in the altered paleochannels, indicates a decrease in temperature outward from the feeder and suggests that fluids had low sulfidation state (Sverjensky, 1987; Einaudi et al., 2003). The $\delta^{34}S$ values of copper sulfides from the chalcocite group at Tordillos (−18.7 to −7.3‰; Fig. 17) are depleted by 24.8‰ to 37.2‰ relative to the main sulfate source (dissolved evaporite units of the Neuquén Basin, $\delta^{34}S$ + 17.3‰ to +18.5‰; Lo Forte et al., 2005) suggesting sulfides precipitated by biogenic sulfate reduction at temperatures <100 °C (Machel et al., 1995). Most of chalcocite group minerals at Barda González show $\delta^{34}S$ values (−21.3 to −18.9‰; Fig. 17) similar to sulfides from the Tordillos deposit, and depleted by 36.4 to 39.4‰ relative to evaporite sulfate ($\delta^{34}S$ +17.3 to +18.5‰; Lo Forte et al., 2005). In summary, bornite and chalcopyrite formed at temperature >100 °C close to the feeder zone and chalcocite group minerals precipitated outward in pore spaces of sandstones at lower temperatures (<100 °C) by TSR and BSR, respectively, of sulfate transported by the incoming mineralizing brines. However, a local source of sulfate could be provided by earlier formed barite. The good correlation between the highest Cu grades and the U and Mo anomalies, suggests these two metals precipitated along with Cu sulfides during the redox reaction. The absence of U, Mo, Pb, Zn anomalies at El Porvenir deposit located south of the Huincul High (see Rainoldi et al., 2019) may be due to the fact that this E-W structure divided the Neuquén Basin in two different compartments (north and the south regions) for basinal fluids migration.

Final exhumation of the Neuquén Group deposits during the Late Miocene-Pliocene (Rodríguez et al., 2007) resulted in partial erosion of mineralized layers and the infiltration of the meteoric water that resulted in the oxidation of the sulfides producing the widespread supergene Fe—Cu, V and U minerals (Fig. 18C). This episode developed under relatively neutral conditions (Sillitoe, 2005) as is evidenced by the lack of any supergene enrichment. Infiltration of meteoric waters in the Lajas Formation at Aguada Baguales promoted partial oxidation of sulfides which caused a decrease in the pH and the replacement of previous clay minerals by kaolinite (beidellite; Fig. 18B).

Sverjensky (1987) propose that the evolution of a reduced oil field brine to an oxidized brine as may be responsible for formation of base metals sediment hosted deposits. At the Huincul High our study shows that at least two stages were necessary: 1) an early hydrocarbon + brine migration through the siliciclastic rocks and its alteration and 2) a later input of warm, oxidized metal and sulfur bearing brines and its interaction with the reservoir rocks or carrier beds (Fig. 18). Similar conclusions were obtained by Rainoldi et al. (2019) for two Cu deposits from other region of the Neuquén Basin consistent with the model proposed by Muchez et al. (2019) for the Neoproterozoic Cu deposits from the Zambian Copper Belt although in this case, the H_2S was sourced from hydrocarbon reservoir rocks.

6. Conclusions

This study reveals the complex relationship between the tectonic evolution of the Neuquén Basin, migration of hydrocarbon and formation waters coupled with the circulation of basinal fluids through black shales, red beds and evaporites involved in the development of both Zn—Pb and Cu mineralization within Mesozoic rocks located north of the Huincul High.

During the Early Cretaceous, hydrocarbon and formation water migration from the Los Molles Formation source rocks to the Lajas Formation reservoir rocks took place after the development of diagenetic quartz overgrowths, fluids exploiting the remaining porosity of the sandstone. Marcasite and illite + illite-smectite mixed layers minerals formed from co-existing brine and hydrocarbons fluids.

Later migration of oxidized basinal brines triggered by Andean tectonism, leached Zn and Pb from the underlying Los Molles Formation black shale and sourced S from evaporites. These brines then entered the Lajas Formation hydrocarbon reservoir, resulting in the precipitation of sphalerite and galena between 119 and 123 °C with siderite as the by-product of TSR and marcasite replaced by sphalerite.

Hydrocarbons and formation waters migration through the shallowest red beds of the Neuquén Group resulted in the bleaching of rocks and the precipitation of pyrite, marcasite, by BSR, and clay coating minerals and quartz overgrowth with barite close to the feeder zones at temperatures of 91–120 °C, mixing fluids confirmed by the wide salinity range of fluid inclusions (1.5–10 wt% NaCl equiv.). Multistage calcite cements formed through pulses of hydrocarbon + formation water migration via oxidation during progressive reaction with the red beds at a wide range of temperatures (100–185 °C).

During subsequent, presumed Miocene tectonic events, basinal brines could have leached Cu from the underlying thick red bed sequences of the basin and remobilized some Zn—Pb from the Lajas Formation. This metalliferous brine entered the hydrocarbon reservoirs resulting in the precipitation of chalcopyrite and bornite close to the feeder zones by TSR and chalcocite group minerals outwards by BSR, along permeable lithologies of the Huincul and Portezuelo formations.

Our results help to explain the distribution of base metals in the Huincul High region and offer a model that can be used to evaluate the metal potential in other areas of the Neuquén Basin and extrapolated to similar geological systems.

CRediT authorship contribution statement

M. Josefina Pons: Conceptualization, Funding acquisition, Formal analysis, Investigation, Methodology, Project administration, Visualization, Writing – original draft, Writing – review & editing. **Marta Franchini:** Conceptualization, Funding acquisition, Formal analysis, Investigation, Methodology, Project administration, Visualization, Writing – review & editing. **Ana L. Rainoldi:** Formal analysis, Visualization, Writing – review & editing. **Adolfo Giusiano:** Formal analysis, Visualization, Investigation, Writing – review & editing. **Nora N. Cesaretti:** Formal analysis, Visualization, Investigation, Writing – review & editing. **Aldo O. Montagna:** Investigation, Writing – review & editing. **Richard Herrington:** Writing – review & editing.

Declaration of competing interest

The authors declare that they have no known competing financial interests or personal relationships that could have appeared to influence the work reported in this paper.

Acknowledgements

The authors are grateful to the editor Dr. Albanese and anonymous reviewers for their valuable and insightful reviews that greatly improved this manuscript. The authors are grateful to Pluspetrol, YPF S.A., Orión del Sur S. A. companies for allowing access to subsurface information and samples. We are especially grateful to Victoria Grosso and Ariel Testi for site access, logistic support, and help during the field work and to Dr. Clemente Recio Hernández and Dr. Adrian Boyce for their collaboration and support during stable isotope analyses. To Dr. Patricia Patrier for her cooperation in some SEM-EDS analyses. This contribution forms part of a several projects financed by Consejo Nacional de Investigaciones Científicas y Técnicas, Argentina (PIP no. 6043, PIP no. 1083, and PUE-2018-229 20180100031CO), Agencia Nacional de Promoción de la Investigación, el Desarrollo Técnico y la Innovación, Fondo para la Investigación Científica y Tecnológica, Argentina (Pict-2010-2608, Pict-prh 2008-00093, and Pict-2008-1120) Acmelab-IoStipend-2009, Universidad Nacional del Comahue, Argentina (nos. 04/I167 and 04/I002), and a support from European Union through an Erasmus Mundus mobility for EU and non-EU scholars-IMACS program (2012-214 edition). RH acknowledges support from NERC Highlight Topic Grant CuBES NE/T002921/1.

Appendix A. Supplementary data

Supplementary data to this article can be found online at https://doi.org/10.1016/j.gexplo.2021.106778.

References

Aguirre, C., Blanco, S., Corbari, S., Ferraresi, P., Schelotto, Rodríguez, 1997. Pluspetrol-Sondeo Pp-Nq.AB-1010 1° y 2° corona (Aguada Baguales). Estudio Sedimentológico Mineralógico y de Microscopía Electrónica, 80p.

Aguirre-Urreta, M.B., Tunik, M., Naipauer, M., Pazos, P.J., Ottone, E.G., Fanning, M.C., Ramos, V.A., 2011. Malargüe Group (Maastrichtian–Danian) deposits in the Neuquén Andes, Argentina: implications for the onset of the first Atlantic transgression related to Western Gondwana break-up. Gondwana Res. 19 (2), 482–494. https://doi.org/10.1016/j.gr.2010.06.008.

de Barrio, R.E., Etcheverry, R.O., Del Blanco, M.A., Domínguez, E.A., Recio Hernández, C., Escobar, R.I., Salvioli, M.A., 2014. Nuevos datos y esquemas genéticos de los depósitos barítico-celestínicos vinculados a la secuencia Jurásico-Cretácica de la Cuenca Neuquina en la Provincia del Neuquén. Rev. Asoición Geol. Argent. 71, 184–200.

Bodnar, R.J., 1992. Revised equation and table for freezing point depressions of H_2O-salt fluid inclusions. In: (Abstracts): PACROFI IV, Fourth Biennal Pan-American Conference on Research of Fluid Inclusions, Program and Abstracts, Lake Arrowhead, CA, 4, p. 15.

Borisenko, A.S., 1977. Study of the salt composition of solutions in gas-liquid inclusions in minerals by the cryometric method. Sov. Geol. Geophys. 18, 11–19.

Burrus, R.C., 1981. Hydrocarbon fluid inclusions in studies on sedimentary diagenesis. In: Hollister, L.S., Crawford, M.L. (Eds.), Fluid Inclusions: Aplications to Petrology. Mineralogical Association of Canadá Short Course Handbook, 6, pp. 138–154.

Casadío, S., Montagna, A.O., 2015. Estratigrafía de la Cuenca Neuquina. In: Ponce, J.J., Montagna, A.O., Carmona, N. (Eds.), Geología de la Cuenca Neuquina y sus sistemas petroleros. Una mirada integradora desde los afloramientos al subsuelo. Fundación YPF – Universidad Nacional de Río Negro, Ciudad Autónoma de Buenos Aires, pp. 8–22.

Catling, D.C., Moore, J., 2003. The nature of coarse-grained crystalline hematite and its implications for the early environment of Mars. Icarus 165, 277–300. https://doi.org/10.1016/S0019-1035(03)00173-8.

Cesaretti, N., Gómez, C., Garrido, M., Domínguez, E., 2002. Fluidos orgánicos asociados a una mineralización de tipo MVT en la Cuenca Neuquina. Formación Lajas. In: Actas del XV Congreso Geológico Argentino. El Calafate, 2, pp. 427–431.

Cevallos, M.F., 2005. Análisis estratigráficos de alta frecuencia del límite Kimmeridgiano-tithoniano en el subsuelo de la Dorsal de Huincul, Cuenca Neuquina. Petrotecnia 12 (2005) pp.55.

Charrier, R., Pinto, L., Rodríguez, M.P., 2007. Tectonostratigraphic evolution of the Andean Orogen in Chile. In: Moreno, T., Gibbons, W. (Eds.), The Geology of Chile. The Geological Society, Special Publication, London, Bath, United Kingdom, pp. 21–114.

Coleman, M.L., Moore, M.P., 1978. Direct reduction of sulfates to sulfur dioxide for isotopic analysis. Anal. Chem. 50, 1594–1595. https://doi.org/10.1021/ac50033a056.

Collins, P.L.F., 1979. Gas hydrates in CO_2-bearing fluid inclusions and the use of freezing data for estimation of salinity. Econ. Geol. 74, 1435–1444. https://doi.org/10.2113/gsecongeo.74.6.1435.

Cooke, D.R., Bull, S.W., Large, R.S., McGoldrick, P.J., 2000. The importance of Oxidized brines for the formation of Australian proterozoic stratiform sediment-hosted PbZn (Sedex) deposits. Econ. Geol. 95, 1–18 doi:0361-0128/00/3019/118.

Coppo, R., Gatica, C., Montagna, A.O., Santiago, E., Valenzuela, G., Wagner, F., 2018. Yacimiento Cupen Mahuida (Formación Lajas), Los reservorios de arenas compactas del Grupo Cuyo. In: Schiuma, M., Hinterwmmer, G., Veragni, E. (Eds.), Rocas reservorios de las secuencias productivas de la Argentina. IAPG, Ciudad Autónoma de Buenos Aires, pp. 427–442.

Cruz, E.C., Boll, A., Gómez Omil, R., Martínez, E.A., Arregui, C., Gulisano, C., Laffitte, G. A., Villar, H.J., 2002. Hábitat de hidrocarburos y sistemas de carga Los Molles y Vaca Muerta en el sector Central de la Cuenca Neuquina. Argentina. In: V Congreso de Exploración y Desarrollo de Hidrocarburos, Mar del Plata, 2002. IAPG (CD-ROM).

Einaudi, M.T., Hedenquist, J.W., Inan, E.E., 2003. Sulfidation state of fluids in active and extinct hydrothermal systems: transitions from porphyry to epithermal environments. In: Simmons, S.F., Graham, I. (Eds.), Volcanic, Geothermal and Ore-forming fluids: Rulers and Witnesses of Processes Within the Earth, Economic Geology Special Publication, 10 (343 p., Boulder).

El Desouky, H.A., Muchez, P., Boyce, A.J., Schneider, J., Cailteux, J.L.H., Dewaele, S., von Quadt, A., 2010. Genesis of sediment-hosted stratiform copper–cobalt mineralization at Luiswishi and Kamoto, Katanga Copperbelt (Democratic Republic of Congo). Mineral. Deposita 45, 735–763. https://doi.org/10.1007/s00126-010-0298-3.

England, W.A., Mackenzie, A.S., Mann, D.M., Quigley, T.M., 1987. The movement and entrapment of petroleum fluids in the subsurface. J. Geol. Soc. Lond. 144, 327–347. https://doi.org/10.1144/gsjgs.144.2.0327.

Escobar, R.I., 2016. Geología y génesis de las mineralizaciones Barito-Celestínicas asociadas a la secuencia cretácina entre las localidades de Bajada del Agrio y Chos Malal, provincia de Neuquén. PhD thesis. Facultad de Ciencias Naturales y Museo, Universidad Nacional de La Plata, Argentina, pp. 208.

Faure, G., 1986. Oxygen and hydrogen in the lithosphere. In: Principles of Isotope Geology. John Wiley Sons, Inc., New York, pp. 460–484.

Garrido, M., Domínguez, E., Gómez, M.C., Cesaretti, N., Aliotta, G., 2000. Una mineralización de Zn-Pb de tipo MVT en la Cuenca Neuquina. In: V Congreso de Mineralogía y Metalogenía. La Plata, pp. 164–170.

George, S.C., Ruble, T.E., Dutkiewicz, A., Eadington, P.J., 2001. Assessing the maturity of oil trapped in fluid inclusions using molecular geochemistry data and visually-determined fluorescence colours. Appl. Geochem. 16, 451–473. https://doi.org/10.1016/S0883-2927 (00)00051-2.

Giusiano, A., Franchini, M., Impiccini, A., O'Leary, S., 2006. Mineralización de Cu asociada a bitumen en las areniscas cretácicas, prospecto Barda González, Neuquén, Argentina. In: XI Congreso Geológico Chileno, Actas 2. Antofagasta, pp. 255–258.

Giusiano, A., Franchini, M., Impiccini, A., Pons, M.J., 2008. Mineralización de Cu en sedimentitas mesozoicas y hábitat de los hidrocarburos en la Dorsal de Huincul, Neuquén. In: XVII Congreso Geológico Argentino. Simposio Cuenca Neuquina. Actas, pp. 769–770.

Goldstein, R.H., Reynolds, T.J., 1994. Systematics of fluid inclusions in diagenetic minerals. In: SEPM Short Course Handbook, p. 31.

Goméz, Omil R., Giorgetti, M., Borchi, P., 2017. El Grupo Cuyo en la Cuenca Neuquina, (Engolfamiento y Dorsal de Huincul, Modelo sedimentario y sistema petrolero). In: XX Congreso Geológico Argentino, Actas, San Miguel de Tucumán, S2, pp. 50–64.

Groeber, P., 1946. Observaciones geológicas a lo largo del meridiano 70°. Hoja Chos Malal. Revista de la Sociedad Geológica Argentina 65, 278–292.

Hahn, G.A., Thorson, J.P., 2006. Geology of the Lisbon Valley sandstone-hosted disseminated copper deposits, San Juan County. In: Bon, R.L., Gloyn, R.W., Park, G. M. (Eds.), Utah. Geological Association Publication, Utah, pp. 511–533.

Hair, A., Hladikova, J., Smejkal, V., 1973. Procedure of direct conversion of sulfates into SO_2 for mass spectrometric analysis of sulfur. Isotope Praxis 18, 433–436.

Hall, G.E.M., Pelchat, J., Loop, 1988. Separation and recovery of various sulphur species in sedimentary rocks for stable sulphur isotopic determination. Chem. Geol. 67, 35–45.

Hanor, J.S., 2000. Barite-celestine geochemistry and environments of formation. Rev. Mineral. Geochem. 40 (1), 193–275. https://doi.org/10.2138/rmg.2000.40.4.

Haynes, D.W., Bloom, M.S., 1987. Stratiform copper deposits hosted by low-energy sediments: IV. Aspects of sulfide precipitation. Econ. Geol. 82, 876–893 hhtps//doi.org/0361-0128/87/667/635-14.

Hitzman, M., Kirkham, R., Broughton, D., Thorson, J., Selly, D., 2005. The sediment-hosted stratiform copper ore system. In: Hedenquist, J.W., JFH, Thompson, Goldfarb, R.J., Richards, J.P. (Eds.), Economic Geology 100th Anniversary Volume, Littleton, pp. 609–642.

Howell, J.A., Schwarz, E., Spalletti, L.A., 2005. The Neuquén Basin: an overview. In: Veiga, G.D., Spalletti, L.A., Howell, J.A., et al. (Eds.), The Neuquén Basin, Argentina: A Case Study in Sequence Stratigraphy and Basin Dynamics, Geological Society, London, Special Publication, 252, p. 114.

Kelley, S.P., Fallick, A.E., 1990. High precision spatially resolved analysis of $\delta^{34}S$ in sulfide using a laser extraction technique. Geochim. Cosmochim. Acta 54, 883–888.

Kesler, S.E., Torsten, W.V., Frederickson, C., Breithaupt, A., Vazquez, R., Furman, F.C., 1997. Hydrogen and oxygen isotope evidence for origin of MVT-forming brines,

southern Appalachians. Geochim. Cosmochim. Acta 61 (7), 1513–1523. https://doi.org/10.1016/S0016-7037(97)00014-8.
Kiyosu, Y., 1973. Sulfur isotope fractionation among sphalerite, galena and sulfide ions. Geochem. J. 7, 191–199.
Larter, S., Huang, H., Adams, J., Bennett, B., Jokanola, O., Oldenburg, T., Jones, M., Head, I., Riediger, C., Fowler, M., 2006. The controls on the composition of biodegraded oils in the deep subsurface: part II—geological controls on subsurface biodegradation fluxes and constraints on reservoir-fluid property prediction. AAPG Bull. 90, 921–938. https://doi.org/10.1306/01270605130.
Leanza, H., 2003. Las sedimentitas huitrinianas y rayosianas (Cretácico inferior) en el ámbito central y meridional de la cuenca Neuquina, Argentina. In: Servicio Geológico Minero Argentino, Serie Contribuciones Técnicas-Geología, 2, Buenos Aires, p. 31.
Leanza, H., Hugo, C., Repol, D., González, R., Danieli, J., 2005. Hoja Geológica 3969-I Zapala, Provincia del Neuquén, vol. 275. Instituto de Geología y Recursos Minerales, Servicio Geológico Minero Argentino, Boletín, Buenos Aires, pp. 1–128.
Leanza, H.A., 1973. Estudio sobre los cambios faciales de los estratos limítrofes Jurásico-Cretácicos entre Loncopué y Picún Leufú, Prov. del Neuquén, Rep. Argentina. Rev. Asoc. Geol. Argent. 28, 97–132.
Leanza, H.A., 1992. Estratigrafía del Paleozoico y Mesozoico anterior a los Movimientos Intermálmicos en la comarca del Cerro Chachil, provincia del Neuquén, Argentina. Rev. Asoc. Geol. Argent. 45 (3–4), 272–299.
Leanza, H.A., Sattler, F., Martinez, R.S., Carbone, O., 2011. La Formación Vaca Muerta y equivalentes (Jurásico Tardío–Cretácico Temprano) en la Cuenca Neuquina. In: Leanza, H.A., Arregui, C., Carbone, O., Danieli, J.C., Vallés, J.M. (Eds.), Geología y Recursos Naturales de la Provincia de Neuquén. Relatorio del VXIII Congreso Geológico Argentino, Buenos Aires, pp. 113–129.
Legarreta, L., Uliana, M.A., 1999. El Jurásico y Cretácico de la Cordillera Principal y la cuenca Neuquina: Facies sedimentarias. In: Caminos, R. (Ed.), Geología Argentina, vol. 29. Servicio Geológico y Minero Argentino, Buenos Aires, pp. 399–416.
Legarreta, L., Cruz, C., Vergani, G., Laffitte, G., Villar, H., 2003. Source rocks, reserves and resources in the Neuquén Basin, Argentina: mass balance approach and exploratory potential. AAPG Bull. 87, 1–10.
Liu, S., Li, Y., Liu, J., Shi, Y., 2015. First-principles study of sulfur isotope fractionation in pyrite-type disulfides. Am. Mineral. 100, 203–208. https://doi.org/10.2138/am-2015-5003.
Lo Forte, G.L., Orti, F., Rosell, L., 2005. Isotopic characterization of Jurassic evaporites. Aconcagua-Neuquén Basin, Argentina. Geol. Acta 3, 155–161. http://hdl.handle.net/20.500.12110/paper_16956133_v3_n2_p155_LoForte.
Lydon, J.W., 1983. Chemical parameters controlling the origin and deposition of sediment-hosted stratiform lead-zinc deposits. In: Mineralogical Association of Canada Short Course Handbook, 8, pp. 175–250.
Lyons, W., 1999. Las areniscas cupríferas del Neuquén. En Zappettini E. (ed.) Recursos Minerales de la República Argentina, Instituto de Geología y Recursos Minerales, SEGEMAR, Anales 35, Buenos Aires, pp. 1149–1158.
Machel, H.G., 1987. Some aspects of diagenetic sulphate-hydrocarbon redox-reactions. In: Marshall, J.D. (Ed.), Diagenesis of Sedimentary Sequences, Geological Society Special Publication, 36, London, pp. 15–28.
Machel, H.G., 1989. Relationships between sulphate reduction and oxidation of organic compounds to carbonate diagenesis, hydrocarbon accumulations, salt domes, and metal sulphide deposits. Carb. Evap. 4, 137–151.
Machel, H.G., 2001. Bacterial and thermochemical sulfate reduction in diagenetic settings—old and new insights. J. Sediment. Geol. 140, 143–175. https://doi.org/10.1016/S0037-0738(00)00176-7.
Machel, H.G., Krouse, H.R., Sassen, R., 1995. Products and distinguishing criteria of bacterial and thermochemical sulfate reduction. Appl. Geochem. 10, 373–389. https://doi.org/10.1016/0883-2927(95)00008-8.
Malone, P., Saavedra, C., Vergani, G., Ferrero, J.C., Limeres, M., Schiuma, M., 2002. Los reservorios del Grupo Cuyo Superior. In: Schiuma, M., Hinterwimmer, Vergani, G. (Eds.), Rocas reservorios de las cuencas productivas de la Argentina. IAPG, Buenos Aires, pp. 277–302.
McCrea, J.M., 1950. On the isotopic chemistry of carbonates and a paleotemperature scale. J. Chem. Phys. 18, 849–857. https://doi.org/10.1063/1.1747785.
Montagna, A.O., Santiago, E., Coppo, R., Rodríguez, E., Meisinger, V., Ponce, J.J., 2017. Algunas consideraciones sobre las heterogeneidades litológicas, granulométricas y petrofísicas de la Formación Lajas y su relación con perfiles eléctricos de pozos. In: XX Congreso Geológico Argentino, Actas, San Miguel de Tucumán, Sesión Técnica 7, pp. 83–90.
Mosquera, A., Ramos, V.A., 2006. Intraplate deformation in the Neuquén Embayment. In: Kay, S.M., Ramos, V.A. (Eds.), Evolution of an Andean Margin: A Tectonic and Magmatic View from the Andes to the Neuquén Basin (35°–39°S Lat): Geological Society of America, Special Paper 407, pp. 97–123.
Mosser-Ruck, R., Cathelineau, M., Guillaume, D., Charpentier, D., Rousset, D., Barres, O., Michau, N., 2010. Effects of temperature, pH and iron/clay and liquid/clay ratios on experimental conversion of dioctahedralsemectite to berthierine, chlorite, verminculite or saponite. Clay Clay Miner. 58 (2), 280–291. https://doi.org/10.1346/CCMN.2010.0580212.
Muchez, P., Minnen, M., Dewaele, S., Hulsbosch, N., 2019. The geology of Mufulira deposit: implications for the metallogenesis of arenite-hosted ore deposits in the Central African Copperbelt. In: Decrée, Robb (Eds.), Ore Deposits: Origin, Exploration, and Exploitation, Geophysical Monograph, First edition. American Geophysical Union, p. 242.
Murowchick, J.B., Barnes, H.L., 1986. Marcasite precipitation from hydrothermal solutions. Geochim. Cosmochim. Acta 50, 2615–2629.
O'Neil, J.R., Clayton, R.N., Mayeda, T.K., 1969. Oxygen isotope fractionation in divalent metal carbonates. J. Chem. Phys. 51, 5547–5558. https://doi.org/10.1063/1.1671982.
Orión del Sur, S.A., 2008. Exploration internal report 2008. In: Orión del Sur SA, Depósitos de cobre sedimentario del Grupo Neuquén Minas Yaraví Norte, La Cuprosa, La Barrosa y La Nuestra, Barda González-Sierra Barrosa. Departamento Confluencia-Provincia del Neuquén, República Argentina, Informe Geológico (Relevamiento de Prospección), 58 p.
Orr, W.L., 1977. Geologic and geochemical controls on the distribution of hydrogen sulfide in natural gas. In: Campos, R., Goni, J. (Eds.), Advances in Organic Geochemistry. Enadisma, Madrid, pp. 571–597.
Ostera, H., García, A.R., Malizia, D., Kokot, P., Wainstein, L., Ricciutti, M., 2016. Shale gas plays, Neuquén Basin, Argentina: chemostratigraphy and mud gas carbon isotopes insights. Braz. J. Geol. 46 (Suppl. 1), 181–196. https://doi.org/10.1590/2317-4889201620150001.
Paz, M., Pons, M.J., Giusiano, A., Cábana, C., Franchini, M., González, E., Impiccini, A., Rainoldi, A.L., 2016. La relación entre la mineralización de Cu y bitumen en el Prospecto La Cuprosa. Rev. Asoc. Geol. Argent. 73 (4), 563–581.
Ploszkiewicz, J.V., Orchuela, I.A., Vailard, J.C., Viñes, R.F., 1984. Compresión y desplazamiento lateral en la zona de Falla Huincul. Estructuras asociadas Provincia del Neuquén. In: IX Congreso Geológico Argentino, Actas 2, Buenos Aires, pp. 163–169.
Pons, M.J., Franchini, M.B., Giusiano, A., Impiccini, A., Godeas, M., 2009. Alteraciones, mineralización de Cu y Bitumen en areniscas Cretácicas del Prospecto Barda González, Neuquén, Argentina. Rev. Asoc. Geol. Argent. 64 (3), 321–333.
Pons, M.J., Rainoldi, A., Franchini, M.B., Beaufort, D., Impiccini, A., Cessartti, N., Giusiano, A., Patrier, P., 2015. Mineralogical signature of hydrocarbon circulation in cretaceous red beds of the Barda González area, Neuquén Basin. AAPG Bull. 99 (3), 525–554. https://doi.org/10.1306/08131413170.
Pons, M.J., Franchini, M., Giusiano, A., Patrier, P., Beaufort, D., Impiccini, A., Rainoldi, A.L., Meinert, L., 2017. Alteration halos in the Tordillos sediment-hosted copper deposit of the Neuquén Basin, Argentina. Ore Geol. Rev. 80, 691–715. https://doi.org/10.1016/j.oregeorev.2016.06.011.
Pradeep, K.A., Fuller, M.E., Gurgas, M.M., Manning, J.F., Dillon, M.A., 1997. Use of stable oxygen and carbon isotope analyses for monitoring the pathways and rates of intrinsic and enhaced in situ biodegradation. Environ. Sci. Technol. 31, 590–596.
Quarisa, D., 2017. Stratigrafia e provenienza di Formazioni Cretaciche del Bacino di Neuquén, Argentina. Master Thesis from. Universita Degli Studi Di Padova, p. 99.
Raggio, M.F., López Pezé, G., Späth, F., Atencio, M., 2014. Modelo de Gas de Centro de Cuenca (Basin-Centered Gas System) en la Formación Lajas. Un desafío exploratorio No Convencional en el ámbito del Engolfamiento Neuquino. In: IX Congreso de Exploración y Desarrollo de Hidrocarburos Simposio de Recursos No Convencionales, Mendoza, pp. 163–185.
Rainoldi, A.L., Franchini, M., Beaufort, D., Impiccini, A., Giusiano, A., Patrier, P., Pons, M.J., 2014. Large-scale bleaching of red beds related to upward migration of hydrocarbons: Los Chihuidos High (37°50′S, 69°27′W), Neuquén Basin, Argentina. J. Sediment. Res. 84 (5), 373–393. https://doi.org/10.2110/jsr.2014.31.
Rainoldi, A.L., Franchini, M., Beaufort, D., Mozley, P., Giusiano, A., Cesaretti, N., Patrier, P., Pons, M.J., 2015. Mineral reaction associated with hydrocarbons paleomigrations in the Huincul High, Neuquén Basin, Argentina. Geol. Soc. Am. Bull. 127, 1711–1729. https://doi.org/10.1130/B31201.1.
Rainoldi, A.L., Franchini, M., Boyse, A.J., Giusiano, A., Cesaretti, N.N., Pons, J., Ríos, J., 2019. Stable isotope and fluid inclusion study of sediment-hosted stratiform copper deposits from the Neuquén Basin, Argentina. Mineral. Deposita 54, 415–436. https://doi.org/10.1007/s00126-018-0815-3.
Ramos, V.A., 1981. Descripción Geológica de la Hoja 33c, Los Chihuidos Norte, Provincia de Neuquén. In: Servicio Nacional Minero Geológico, Boletín, 182, Buenos Aires, p. 103.
Ramos, V.A., 2010. The tectonic regime along the Andes: present-day and Mesozoic regimes. Geol. J. 45, 2–25. https://doi.org/10.1002/gj.
Ramos, V.A., Kay, S.M., 2006. Overview of the tectonic evolution of the southern Central Andes of Mendoza and Neuquén (35°–39°S latitude). In: Kay, S.M., Ramos, V.A. (Eds.), Evolution of an Andean Margin: A Tectonic and Magmatic View From the Andes to the Neuquén Basin (35°–39°S Lat): Geological Society of America Special Paper, 407, pp. 1–17.
Ramos, V.A., Ricardi, A.C., Rolleri, E.O., 2004. Límites Naturales del Norte de la Patagonia. Rev. Asoc. Geol. Argent. 59 (4), 785–786.
Riccardi, A.C., 2008. The marine Jurassic of Argentina: a biostratigraphic framework. Episodes 31 (3), 326–335. https://doi.org/10.18814/epiiugs/2008/v31i3/007.
Riecker, R.E., 1962. Hydrocarbon fluorescence and migration of petroleum. AAPG Bull. 46, 60–75. https://doi.org/10.1306/BC74375B-16BE-11D7-8645000102C1865D.
Robinson, D., Santana de Zamora, A., 1999. The smectite to chlorite transition in Chipilapa geothermal system, El Salvador. Am. Mineral. 84 (4), 607–619. https://doi.org/10.2138/am-1999-0414.
Rodríguez, M.F., Leanza, H.A., Salvarredy Aranguren, M., 2007. Hoja Geológica 3969-II, Neuquén, provincias del Neuquén, Río Negro y La Pampa. Instituto del Geología y Recursos Minerales. Servicio Geológico Minero Argentino, Boletín 370, Buenos Aires, p. 165.
Salvioli, M.A., 2017. Geología y génesis de los depósitos baritico-polimetálicos (Ba-Fe-Pb-Cu-Zn-Mn) del área de Colipilli, sector centro occidental de la Cuenca Neuquina. PhD thesis. Universidad Nacional de La Plata, Facultad de Ciencias Naturales y Museo, p. 256.
Schiuma, M., Saavedra, C., Malone, P., Cevallos, M., Rebori, L., Vergani, G., 2002. Los reservorios del Gupo Lotena. Argentina. In: Schiuma, M., Hinterwimmer, G., Vergani, G. (Eds.), Grupo Lotena, Rocas Reservorios de las Cuencas Productivas de la Argentina, Cuenca Neuquina. IAPG, Buenos Aires, pp. 303–334.

Schwarz, E., Howell, J.A., 2005. Sedimentary evolution and depositional architecture of a low stand sequence set: the Lower Cretaceous Mulichinco Formation, Neuquén Basin, Argentina. In: Veiga, G.D., Spalletti, L.A., Howell, J.A., Schwarz, E. (Eds.), The Neuquén Basin, Argentina: A Case Study in Sequence Stratigraphy and Basin Dynamics, Geological Society Special Publications, 252, pp. 109–138. London.

Seal II, R.R., 2006. Sulfur isotope geochemistry of sulfide minerals. Rev. Mineral. Geochem. 61 (1), 633–677. https://doi.org/10.2138/rmg.2006.61.12.

Sheppard, S.M.F., 1986. Characterization and isotopic variations in natural waters. In: Valley, J.W., Taylor, H.P., O'Neil, J.R. (Eds.), Stable Isotopes in High Temperature Geological Processes, Mineralogical Society of America Reviews in Mineralogy, vol. 16, pp. 165–183.

Sheppard, S.M.F., Gilg, H.A., 1996. Stable isotope geochemistry of clay minerals. Clay Miner. 31, 1–24 https://doi=10.1.1.616.8660&rep=rep1&type=pdf.

Sigismondi, M., Ramos, V., 2009. El flujo de calor en la cuenca Neuquina. Petrotecnia 58–76.

Sillitoe, R.H., 2005. Supergene oxidized and enriched porphyry copper and related deposits. In: Economic Geology 100th Anniversary Volume, pp. 723–768.

Silvestro, J., Zubiri, M., 2008. Convergencia oblicua: Modelo estructural alternativo para la Dorsal neuquina (39° S)-Neuquén. Rev. Asoc. Geol. Argent. 63 (1), 49–64.

Sugimoto, T., Waki, S., Itoh, H., Muramatsu, A., 1996. Preparation of monodisperse platelet-type hematite particles from a highly condensed β-FeOOH suspension. Colloids Surf. A Physicochem. Eng. Asp. 109, 155–165. https://doi.org/10.1016/0927-7757(95)03454-4.

Surdam, R.C., Crossey, L.J., Hagen, E.S., Heasler, H.P., 1989. Organic-inorganic interactions and sandstone diagenesis. AAPG Bull. 73, 1–32.

Sverjensky, D.A., 1987. The role of migrating oil field brines in the formation of sediment-hosted Cu-rich deposits. Econ. Geol. 82, 1130–1141 http://doi.org/0361-0128/87/699/1130-12.

Testi, A., 2006. Informe de avance prospecto Tordillos. In: Orión del Sur S.A.-Minera Agua Rica República Argentina, (inédito), Neuquén, p. 13.

Tunik, M., Folguera, A., Naipauer, M., Pimentel, M.M., Ramos, V.A., 2010. Early uplift and orogenic deformation in the Neuquén Basin: constraints on the Andean uplift from U–Pb and Hf isotopic data of detrital zircons. Tectonophysics 489 (1–4), 258–273. https://doi.org/10.1016/j.tecto.2010.04.017.

Uliana, M.A., Legarreta, L., 1993. Hydrocarbons habitat in a Triassic to Cretaceous sub-andean setting: Neuquén Basin, Argentina. J. Pet. Geol. 16 (4), 397–420. https://doi.org/10.1111/j.1747-5457.1993.tb00350.x.

Veiga, R., 2002. Migración de hidrocarburos y sistemas petroleros cuyanos en el ámbito central de la Cuenca Neuquina – Argentina. In: V Congreso de Exploración y Desarrollo de Hidrocarburos, IAPG, CD Trabajos Técnicos, Mar del Plata, p. 20.

Velde, B., 1985. Clay Minerals: A Physico-Chemical Explanation of their Occurrence: Developments in Sedimentology. In: Developments in sedimentology, , 1st ed.40. Elseiver, Amsterdam, pp. 1–427.

Vergani, G.D., Tankard, A.J., Belotti, H.J., Welsink, H.J., 1995. Tectonic evolution and paleogeography of the Neuquén Basin, Argentina. In: Tankard, A.J., Suárez Soruco, R., Welsink, H.J. (Eds.), Petroleum Basins of South America, American Association of Petroleum Geologists, Memoir, Tulsa, 62, pp. 383–402.

Vicente, J.C., 2005. Dynamic paleogeography of the Jurassic Andean Basin: pattern of transgression and localization of main straits through the magmatic arc. Rev. Asoc. Geol. Argent. 60, 221–250.

Vicente, J.C., 2006. Dynamic paleogeography of the Jurassic Andean Basin: pattern of regression and general considerations on main features. Rev. Asoc. Geol. Argent. 61, 408–437.

Villar, H., Legarreta, L., Cruz, C., Laffite, G., Vergani, G., 2005. Los cinco sistemas petroleros coexistentes en el sector sudeste de la Cuenca Neuquina: Definición geoquímica y comparación a lo largo de una transecta de 150 km. Bol. Inform. Petrol. BIP, Cuarta Época año 2 (3), 50–67.

Vottero, J.A., González, J.M., 2002. Los reservorios de la Formación Mulichinco. In: Schiuma, M., Hinterwimmer, G., Vergani, G. (Eds.), Rocas Reservorios de las cuencas productivas de la Argentina. IAPG, Buenos Aires, pp. 383–400.

Wagner, T., Boyce, A.J., Fallick, A.E., 2002. Laser combustion analysis of $\delta^{34}S$ of sulfosalt minerals: determination of the fractionation systematic and some crystal-chemical considerations. Geochim. Cosmochim. Acta 66 (16), 2855–2863. https://doi.org/10.1016/S0016-7037(02)00891-8.

Yeh, H., 1980. D/H ratios and late-stage dehydration of shales during burial. Geochim. Cosmochim. Acta 44 (2), 341–352.

Yurtsever, Y., Gat, J.R., 1981. Atmospheric waters. In: Gat, J.R., Gonfiantini, R. (Eds.), Stable Isotope Hydrogeology, Deuterium and Oxygen-18 in the Water Cycle. IAEA Technical Report Series, vol. 210, pp. 103–142.

Zamora Valcarce, G., Zapata, T., Del Pino, D., Ansa, A., 2006. Structural evolution and magmaticcharacteristics of the Agrio Fold-and-thrust belt. In: Kay, S.M., Ramos, V.A. (Eds.), Evolution of an Andean Margin: A Tectonic and Magmatic View From the Andes to the Neuquén Basin (35°–39°Lat), Geological Society of America, Special Paper, 407, pp. 125–145.

Zientek, M.L., Wintzer, N.E., Hayes, T.S., Parks, H.L., Briggs, D.A., Causey, J.D., Hatch, S. A., Jenkins, M.C., Williams, D.J., 2015. Qualitative assessment of selected areas of the world for undiscovered sediment-hosted stratabound copper deposits. In: U.S. Geological Survey Scientific Investigations Report 2010-5090-Y, p. 143.